# A variational multiscale stabilized finite element formulation for Reissner-Mindlin plates and Timoshenko beams

A. Aguirre[a,b], R. Codina[a], J. Baiges[a]
[a] Universitat Politècnica de Catalunya, Jordi Girona 1 − 3, Edifici C1, Barcelona 08034, Spain.
[b] Universidad de Santiago de Chile, Av. Libertador Bernardo O'Higgins 3363, Estación Central, Santiago, Chile.
alejandro.aguirre@upc.edu (A. Aguirre), ramon.codina@upc.edu (R. Codina), joan.baiges@upc.edu (J. Baiges)

**Abstract**

The theories for thick plates and beams, namely Reissner-Mindlin's and Timoshenko's theories, are well known to suffer numerical locking when approximated using the standard Galerkin finite element method for small thicknesses. This occurs when the same interpolations are used for displacement and rotations, reason for which stabilization becomes necessary. To overcome this problem, a Variational Multiscale stabilization method is analyzed in this paper. In this framework, two different approaches are presented: the Algebraic Sub-Grid Scale formulation and the Orthogonal Sub-Grid Scale formulation. Stability and convergence is proved for both approaches, explaining why the latter performs much better. Although the numerical examples show that the Algebraic Sub-Grid Scale approach is in some cases able to overcome the numerical locking, it is highly sensitive to stabilization parameters and presents difficulties to converge optimally with respect to the element size in the $L^2$ norm. In this regard, the Orthogonal Sub-Grid Scale approach, which considers the space of the sub-grid scales to be orthogonal to the finite element space, is shown to be stable and optimally convergent independently of the thickness of the solid. The final formulation is similar to approaches developed previously, thus justifying them in the frame of the Variational Multiscale concept.

*Keywords:* `Reissner-Mindlin Plate, Timoshenko Beam, Shear Locking, Variational Multiscale`.

## 1 Introduction

In the context of computational mechanics, plates and beams are structural elements that are able to represent three dimensional objects in which the length of one or two of its dimensions is significantly smaller than the others. This dimensional reduction allows engineers to model complex structures at the cost of introducing rotations as independent variables. The Reissner-Mindlin equations are commonly used to describe the behavior of thin and moderately thick plates under transverse loads. This model differs from the Poisson-Kirchhoff equations for thin plates by considering the shear deformations due to distortion. In a physical sense, it is assumed that a straight line normal to the undeformed middle plane will remain straight but not necessarily perpendicular to the middle plane after deformation. The same analogy applies

to the Timoshenko equations for thin-thick beams, with respect to the Euler-Bernoulli equations for thin beams. This leads to two groups of equations: the thin-thick theories, referred to as Reissner-Mindlin plates and Timoshenko beams, and the thin theories, referred to as Poisson-Kirchhoff plates and Euler-Bernoulli beams.

This paper is focused on the Finite Element (FE) stabilization of thin-thick theories of plates and beams, founded on the fact that applications in engineering usually fall into this category, and in the interest of using $C^0$ interpolations for displacement and rotations that are not possible using thin theories. In this context, both in Reissner-Mindlin plate and Timoshenko beam theories, the thickness of the structure appears explicitly in the partial differential equations, which results in a dominance of the shear term as it tends to the slender limit case. This fact together with the zero shear strain constraint leads to *numerical locking* when the equations are solved using the same interpolation for deflection and rotations, and it is the reason it needs to be stabilized. In the case of beams, the way locking occurs can be explicitly analyzed from the stiffness matrix of the elements [1].

A considerable amount of work has been put into the design of *locking-free* elements, namely that the order of convergence does not depend on the thickness of the structure. The existing approaches can be classified depending on whether or not the problem is dealt with in the irreducible form or if the shear strain is interpolated as an additional variable of the problem, which alleviates the zero shear constraint. In the irreducible approach, the equations are presented in terms of deflections and rotations only, and if these equations are discretized using standard polynomial spaces, the numerically simulated structure behaves with a stiffness larger than it should for small thicknesses [2]. This pure numerical response is known as numerical locking, and for this particular case, it is often called *shear-locking* because it occurs due to the inability to reproduce a zero shear strain field. In that regard, the numerical locking will occur for any loading that results in a pure bending state of the structure. On the other hand, the mixed formulation approach consists in interpolating the shear strain from the constitutive equations as an additional unknown. This can be extended, although not necessarily, to the dual-mixed formulation by also interpolating the bending strain. This type of implementations is used to avoid restrictive constraints; however, they are inf-sup deficient and also require stabilization. For a better understanding of the FE approach to plates the reader can refer to [3, 4].

The most common approach used to solve the problem, independently of which variables are interpolated, is to use MITC (Mixed Interpolation of Tensorial Components) elements, that allows one to use different interpolations for each unknown. These approaches have been, and are still being developed for different types of problems [5, 6]. The reader can refer to [7] for a general overview, and also to [8] for a general analysis of the design procedure of MITC elements based on the velocity-pressure pair of the Stokes problem. The main challenge of this approach is to develop a stabilized formulation that converges optimally for every unknown using the lowest possible order of interpolation. A good insight of this in relation to the plate

problem can be followed from [9], where it was established that shear stress is convergent if the bending moment converges at a high enough rate. This led to further developments using a variational approach [10] that was valid for any element of high enough order of interpolation for MITC elements, limited to using at least quadratic interpolations for the displacements. This limitation was improved in [11] by adding some consistent terms to the formulation. This type of elements has also been extended to shells [12], although some sort of stabilization is also required in this framework [13].

A search of the literature shows that another common methodology to treat shear-locking is by using different types of selective integration [14, 15]. This, however, is limited to particular element shapes and element orders (for example for bilinear quads), but it is not a general approach. Stabilization of shear locking can be achieved through many different approaches such as using Lagrange multipliers [16, 17], non-conforming method approaches [18, 19] which have also been a common topic of discussion, or discontinuous Petrov-Galerkin methods [20, 21], to name a few. Another approach was taken in [22], where the dual mixed formulation was stabilized using inter-elemental jumps of the unknowns. This approach provides optimal convergence of all the unknowns using linear interpolations only. A completely different approach was followed in [23], where a locking-free formulation is obtained from general polygonal space discretization rather than from standard finite elements.

Another methodology consists in formulating the stabilization from the multiscale perspective. It started from the introduction of the Galerkin-Least Squares method [10] and was further developed in [24]. Another least-squares type formulation was developed in [25] by introducing stabilization terms using the shear stress computed from the equilibrium equations. A rather different approach was used in [26], where a preconditioner was obtained using a multigrid method that was initially proposed in [27], where a conjugate gradient iterative algorithm was used to solve the linear system. The mixed formulation was also solved in [28] by introducing different interpolations for bending and shear effects. Also, in [29] a method was developed using a modified version of the formulation presented in [30], where an additional term was added to the mixed form. A similar approach to one of the stabilization methods to be described in the following was adopted in [31], in particular applied to the Discrete Shear Gap (DSG) formulation, which was already designed to avoid shear locking.

In this paper, the Reissner-Mindlin plate and the Timoshenko beam problems are addressed using the Variational Multiscale (VMS) method, a framework to develop stabilized formulations originally introduced in [32, 33]. In these formulations, the original Galerkin formulation is modified as little as possible using residual-based terms, making it consistent. The stabilized formulations presented in this paper share some characteristics with other formulations presented in the literature, such as [4, 7, 11]; however, the final outcome is not exactly the same and the motivation to derive the methods we propose is completely different [34].

The paper is organized as follows: A brief overview of the physical problem is presented in section 2 and

the variational form is given in section 3. The general form of the stabilized FE formulation is explained in section 4 and its implementation for the plate and beam problems is presented in section 5. The numerical analysis in which the method is proven to be stable and convergent is presented in section 6 and lastly, numerical results are shown in section 7.

## 2 Continuous boundary value problem

Consider a general definition of the transverse deflection $w$ and the rotation $\boldsymbol{\theta}$ of a structure. In the case of plates, the rotation is a vector that contains the rotations that make it bend in the $x$ and $y$ directions as $\boldsymbol{\theta} = [\theta_x, \theta_y]$. Since the beam problem is a dimensional reduction of the plate problem, a single rotation in the $z$ direction is considered in this case, as $\boldsymbol{\theta} = \theta = \theta_z$. In the problems presented below, the geometries and coordinate systems are defined under the convention presented in Fig. 1. Only beams in the plane will be considered, the extension to 3D beams being straightforward.

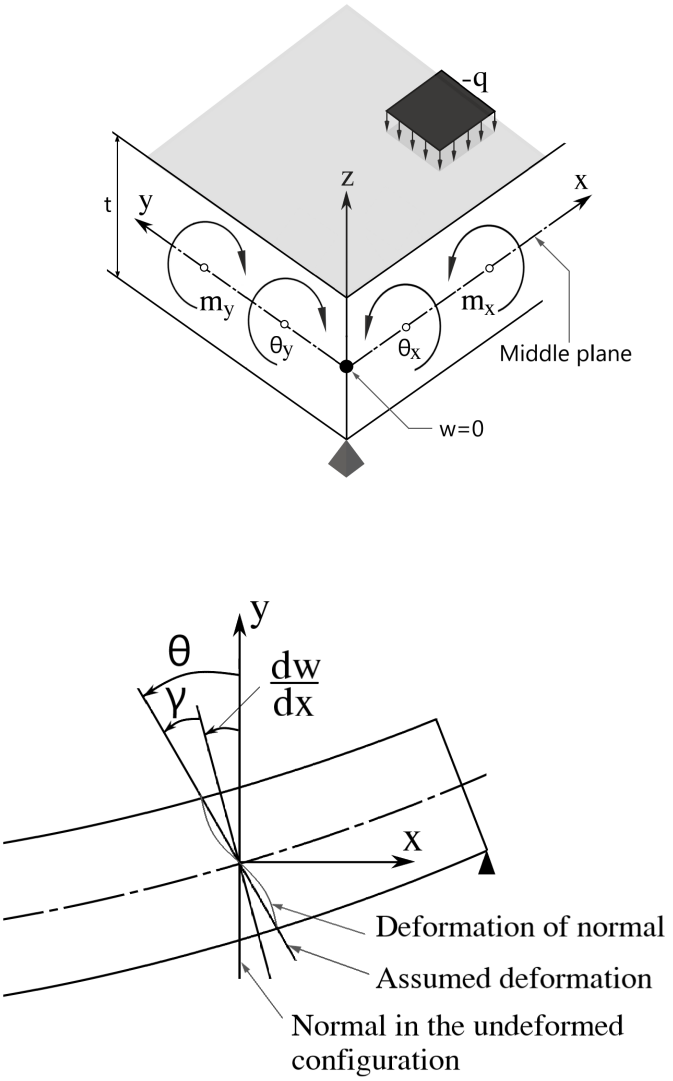


Figure 1: Coordinate system and definition of variables in plates and beams.

Let us define a domain in a general manner as $\Omega$ and its boundary $\Gamma = \partial\Omega$. Then $\Omega$ can be particularized for plates as $\Omega = \Omega_P$ and for beams as $\Omega = \Omega_B$, with their corresponding boundaries $\Gamma_P$ and $\Gamma_B$. The irreducible form of the Reissner-Mindlin plate problem consists in finding $\mathbf{u} = [\boldsymbol{\theta}, w]$ in the domain $\Omega_P$ of $\mathbb{R}^2$ with boundary $\Gamma_P$ as the solution to

$$-k_1\Delta\boldsymbol{\theta} - k_2\nabla(\nabla\cdot\boldsymbol{\theta}) - \frac{1}{\varepsilon}(\nabla w - \boldsymbol{\theta}) = \mathbf{m} \qquad \text{in } \Omega_P, \tag{2.1}$$

$$-\frac{1}{\varepsilon}\nabla\cdot(\nabla w - \boldsymbol{\theta}) = q \qquad \text{in } \Omega_P, \tag{2.2}$$

$$w = 0 \qquad \text{in } \Gamma_P, \tag{2.3}$$

$$\boldsymbol{\theta} = \mathbf{0} \qquad \text{in } \Gamma_P, \tag{2.4}$$

for properly defined external loading moments $\mathbf{m} = [m_x, m_y]$, transverse loads $q$ and

$$k_1 = \frac{Et^3}{24(1+\nu)}, \qquad k_2 = \frac{Et^3}{24(1-\nu)}, \qquad \varepsilon = \frac{2(1+\nu)}{E\kappa t}, \tag{2.5}$$

where $E$ is the Young modulus, $\nu$ the Poisson ratio, $t$ the thickness and $\kappa$ the shear correction factor. In the development presented below, only homogeneous Dirichlet conditions are considered in (2.3) and (2.4), for simplicity. Note that $\varepsilon \to \infty$ as $t \to 0$. However, $k_1$ and $k_2$ are $\mathcal{O}(t^3)$, whereas $\varepsilon^{-1}$ is $\mathcal{O}(t)$. We have used the symbol $\varepsilon^{-1}$ for the shear stiffness to emphasize that it dominates the bending stiffnesses as $t \to 0$.

Similarly, the Timoshenko beam problem consists in finding $\mathbf{u} = [\theta, w]$ defined in the domain $\Omega_B$ of $\mathbb{R}$ with boundary $\Gamma_B$ such that

$$-\frac{d}{dx}\left(EI\frac{d\theta}{dx}\right) - GA^*\left(\frac{dw}{dx} - \theta\right) = m \qquad \text{in} \quad \Omega_B, \tag{2.6}$$

$$-\frac{d}{dx}\left[GA^*\left(\frac{dw}{dx} - \theta\right)\right] = q \qquad \text{in} \quad \Omega_B, \tag{2.7}$$

$$w = 0 \qquad \text{in } \Gamma_B, \tag{2.8}$$

$$\theta = 0 \qquad \text{in } \Gamma_B, \tag{2.9}$$

where $G$ is the shear modulus, $I$ is the inertia in the bending axis, and $A^*$ is the traverse reduced section area of the beam. The equilibrium equations are completed by the external moment, in this case $\boldsymbol{m} = m = m_z$, and external loads $q$. Comparing the beam and the plate equations, it is observed that $EI$ plays the role of $k_1$ and $k_2$, whereas $GA^*$ plays the role of $\varepsilon^{-1}$. Note that indeed both $EI$ and $k_1$, $k_2$ are $\mathcal{O}(t^3)$, whereas $GA^*$ and $\varepsilon^{-1}$ are $\mathcal{O}(t)$, and the later become dominant when $t \to 0$.

It is important to mention that thick theories account for the shear strains $\boldsymbol{\gamma} := \nabla w - \boldsymbol{\theta}$, contrary to the $\boldsymbol{\gamma} = \mathbf{0}$ assumption of thin theories. Nevertheless, thick theories should converge to the corresponding thin theory solution when approaching the thin limit $t \to 0$.

Additional notation is necessary to build the formulations to be described below. Let us define, in a general manner, a linear differential operator $\mathcal{L}$, the trace operator $\mathcal{D}$ that makes the problem well defined, and a external force vector $\mathbf{f}$. Either the plate or beam problems can now be written as: find $\mathbf{u} : \Omega \to \mathbb{R}^n$

such that

$$\mathcal{L}\mathbf{u} = \mathbf{f} \qquad \text{in} \quad \Omega, \tag{2.10}$$

$$\mathcal{D}\mathbf{u} = \bar{\mathbf{u}} \qquad \text{on} \quad \Gamma. \tag{2.11}$$

For the problems we consider, $\mathcal{D}\mathbf{u}$ is just the trace of $\mathbf{u}$ on $\Gamma$. As it has been mentioned, we will take $\bar{\mathbf{u}} = \mathbf{0}$ for simplicity.

We can refer to the Reissner-Mindlin plate problem when $n = 3$, $\mathcal{L} = \mathcal{L}_{\mathrm{RM}}$ and $\mathbf{f} = \mathbf{f}_{\mathrm{RM}}$, given by

$$\mathcal{L}_{\mathrm{RM}}\mathbf{u} = \begin{bmatrix} -k_1\Delta\boldsymbol{\theta} - k_2\nabla(\nabla\cdot\boldsymbol{\theta}) - \frac{1}{\varepsilon}(\nabla w - \boldsymbol{\theta}) \\ -\frac{1}{\varepsilon}\nabla\cdot(\nabla w - \boldsymbol{\theta}) \end{bmatrix}, \qquad \mathbf{f}_{\mathrm{RM}} = \begin{bmatrix} \mathbf{m} \\ q \end{bmatrix}, \tag{2.12}$$

and to the Timoshenko beam problem when $n = 2$, $\mathcal{L} = \mathcal{L}_{\mathrm{T}}$ and $\mathbf{f} = \mathbf{f}_{\mathrm{T}}$, given by

$$\mathcal{L}_{\mathrm{T}}\mathbf{u} = \begin{bmatrix} -\frac{d}{dx}\left(EI\frac{d\theta}{dx}\right) - GA^*\left(\frac{dw}{dx} - \theta\right) \\ -\frac{d}{dx}\left(GA^*\left(\frac{dw}{dx} - \theta\right)\right) \end{bmatrix}, \qquad \mathbf{f}_{\mathrm{T}} = \begin{bmatrix} m \\ q \end{bmatrix}. \tag{2.13}$$

To build the variational method below, it also is necessary to define the flux operator $\mathcal{F}$. Following the same notation as before, the flux operator corresponds to the Reissner-Mindlin problem when $\mathcal{F} = \mathcal{F}_{\mathrm{RM}}$, defined as

$$\mathcal{F}_{\mathrm{RM}}(\mathbf{u}) = \begin{bmatrix} k_1\mathbf{n}\cdot\nabla\boldsymbol{\theta} + k_2\mathbf{n}\nabla\cdot\boldsymbol{\theta} \\ \mathbf{n}\cdot\frac{1}{\varepsilon}(\nabla w - \boldsymbol{\theta}) \end{bmatrix}, \tag{2.14}$$

and to the Timoshenko beam problem when $\mathcal{F} = \mathcal{F}_{\mathrm{T}}$, given by

$$\mathcal{F}_{\mathrm{T}}(\mathbf{u}) = \begin{bmatrix} EI\frac{d\theta}{dx} \\ GA^*\left(\frac{dw}{dx} - \theta\right) \end{bmatrix}. \tag{2.15}$$

## 3 Variational Form

Consider $H^1(\Omega)$ as the space of functions in $L^2(\Omega)$ whose derivatives belong to $L^2(\Omega)$ and $H^1_0(\Omega)$ the subspace of $H^1(\Omega)$ of functions vanishing on $\Gamma$. In both specific problems, we denote the space of the deflection as $\mathcal{V} = H^1_0(\Omega)$; the space of the rotations $\mathcal{Q}$ will correspond to $\mathcal{Q} = H^1_0(\Omega)^2$ when referring to plates and to $\mathcal{Q} = H^1_0(\Omega)$ when referring to beams.

Let us denote by $(\cdot,\cdot)_\Omega$ the $L^2$-inner product and define $\langle\cdot,\cdot\rangle_\Omega$ as the integral of the product of two functions in $\Omega$. We also denote as $\mathcal{X} = \mathcal{V}\times\mathcal{Q}$ the spaces where the weak problem is defined, whose test functions are $\mathbf{v} = [\boldsymbol{\phi}, v] \in \mathcal{X}$. Let us introduce the bilinear form of the problem $B$ and the linear form $L$ as

$$B(\mathbf{u},\mathbf{v}) = \langle\mathcal{L}\mathbf{u},\mathbf{v}\rangle_\Omega + \langle\mathcal{F}\mathbf{u},\mathcal{D}\mathbf{v}\rangle_{\partial\Omega}, \tag{3.1}$$

$$L(\mathbf{v}) = \langle\mathbf{f},\mathbf{v}\rangle_\Omega. \tag{3.2}$$

With all the above, the general problem in (2.10) and (2.11) is equivalent to the weak form of the problem,

which consists in finding $\mathbf{u} \in \mathcal{X}$ such that

$$B(\mathbf{u}, \mathbf{v}) = L(\mathbf{v}), \tag{3.3}$$

for all $\mathbf{v} \in \mathcal{X}$.

## 4 Stabilized Finite Element Formulation

The standard FE discretization consists in taking a finite partition $\{K\}$ of the domain $\Omega$. Let the functional space where the continuous problem is posed be denoted by $\mathcal{X}$ from which the constructed conforming FE space $\mathcal{X}_h$ is a subset. Then the Galerkin FE approximation consists in finding $\mathbf{u}_h \in \mathcal{X}$ such that

$$B\left(\mathbf{u}_h, \mathbf{v}_h\right) = L\left(\mathbf{v}_h\right) \qquad \forall\, \mathbf{v}_h \in \mathcal{X}_h. \tag{4.1}$$

The stabilized formulation analyzed in this paper is constructed in the VMS framework. The idea is to add additional terms to the Galerkin formulation of the problem that enhance stability without upsetting accuracy. This is achieved by splitting the space of unknowns as $\mathcal{X} = \mathcal{X}_h \oplus \mathcal{X}'$, where $\mathcal{X}_h$ is the part that can be solved in the FE space and $\mathcal{X}'$ is the remainder, or sub-grid scale, part. This leads to the splitting of the unknowns $\mathbf{u} = \mathbf{u}_h + \mathbf{u}'$ and test functions $\mathbf{v} = \mathbf{v}_h + \mathbf{v}'$. This splitting modifies the original formulation shown in (4.1) and turns the problem into: find $\mathbf{u}_h \in \mathcal{X}_h$ and $\mathbf{u}' \in \mathcal{X}'$ such that

$$B\left(\mathbf{u}_h, \mathbf{v}_h\right) + B\left(\mathbf{u}', \mathbf{v}_h\right) = L\left(\mathbf{v}_h\right) \qquad \forall\, \mathbf{v}_h \in \mathcal{X}_h, \tag{4.2}$$

$$B\left(\mathbf{u}_h, \mathbf{v}'\right) + B\left(\mathbf{u}', \mathbf{v}'\right) = L\left(\mathbf{v}'\right) \qquad \forall\, \mathbf{v}' \in \mathcal{X}'. \tag{4.3}$$

The way this formulation is constructed requires an approximation of the sub-grid scales to be complete, which will be computed as a function of the FE part, as shown below. Note that choosing $\mathcal{X}' = \{0\}$ yields the Galerkin method, making this method consistent by construction.

### *4.1 Sub-grid scales in the element interiors*

At this point, the approximation requires to solve more variables than the initial problem. This is dealt with by modifying (4.2) by using the additivity of the integral and the identity of the bilinear operator:

$$B\left(\mathbf{u}, \mathbf{v}\right) = \sum_K \langle \mathcal{L}\mathbf{u}, \mathbf{v} \rangle_K + \sum_K \langle \mathcal{F}\mathbf{u}, \mathcal{D}\mathbf{v} \rangle_{\partial K} = \sum_K \langle \mathbf{u}, \mathcal{L}^*\mathbf{v} \rangle_K + \sum_K \langle \mathcal{D}\mathbf{u}, \mathcal{F}^*\mathbf{v} \rangle_{\partial K}\,, \tag{4.4}$$

where the superscript * denotes the adjoint of an operator. In the current problems, the operators involved are self-adjoint, which means that $\mathcal{L}^* = \mathcal{L}$ and $\mathcal{F}^* = \mathcal{F}$; nevertheless, the superscript is left as a reference. In this manner, equation (4.2) can be written as

$$B\left(\mathbf{u}_h, \mathbf{v}_h\right) + \sum_K \left[\left\langle \mathbf{u}', \mathcal{L}^*\mathbf{v}_h \right\rangle_K + \left\langle \mathcal{D}\mathbf{u}', \mathcal{F}^*\mathbf{v}_h \right\rangle_{\partial K}\right] = L(\mathbf{v}_h). \tag{4.5}$$

Then the problem reduces to find a proper approximation for $\mathbf{u}'$. This can be achieved in (4.3) by approximating $\mathbf{u}'$ in terms of $\mathbf{u}_h$. We have that

$$\begin{aligned} B\left(\mathbf{u}', \mathbf{v}'\right) &= L\left(\mathbf{v}'\right) - B\left(\mathbf{u}_h, \mathbf{v}'\right), \\ &= L\left(\mathbf{v}'\right) - \sum_K \left[\left\langle \mathcal{L}\mathbf{u}_h, \mathbf{v}' \right\rangle_K + \left\langle \mathcal{F}\mathbf{u}_h, \mathcal{D}\mathbf{v}' \right\rangle_{\partial K}\right], \\ &= \sum_K \left[\left\langle \mathcal{R}\mathbf{u}_h, \mathbf{v}' \right\rangle_K + \left\langle \mathcal{F}\mathbf{u}_h, \mathcal{D}\mathbf{v}' \right\rangle_{\partial K}\right], \end{aligned} \tag{4.6}$$

where $\mathcal{R}\mathbf{u}_h = \mathbf{f} - \mathcal{L}\mathbf{u}_\mathbf{h}$ is the FE residual. For now let us impose that $\mathcal{D}\mathbf{u}' = \mathbf{0}$ on $\partial K$ in an essential way, making the sub-grid scale test function satisfy $\mathcal{D}\mathbf{v}' = \mathbf{0}$ on $\partial K$. This yields the following approximation

$$\mathbf{u}' = \mathcal{L}^{-1}\left(\mathcal{R}\mathbf{u}_h + \mathbf{v}'^{\perp}\right), \tag{4.7}$$

where $\mathbf{v}'^{\perp}$ guarantees that $\mathbf{u}' \in \mathcal{X}'$. In this expression, $\mathcal{L}^{-1}$ cannot be computed directly, so it is approximated element by element as

$$\mathbf{u}'\,|_K \approx \boldsymbol{\tau}_K \left(\mathcal{R}\mathbf{u}_h + \mathbf{v}'^{\perp}\right)|_K, \tag{4.8}$$

where $\boldsymbol{\tau}_K$ is a matrix that approximates $\mathcal{L}^{-1}$ on each element $K$. The function $\mathbf{v}'^{\perp}$ depends on the space of the sub-grid scales, so it can be written in a general form as

$$\mathbf{u}'\,|_K \approx \boldsymbol{\tau}_K P'\left(\mathcal{R}\mathbf{u}_h\right)|_K, \tag{4.9}$$

where $P'$ is the $L^2$ projection onto the sub-grid scale space $\mathcal{X}'$ and $P' = I - P'^{\perp}$, with $I$ being the identity in $\mathcal{X}$. This approximation allows us to rewrite the modified version of the problem in (4.5) as a function of the FE variables, making the number of unknowns to be the same as the original problem, as follows

$$B\left(\mathbf{u}_h, \mathbf{v}_h\right) + \sum_K \left\langle \boldsymbol{\tau}_K P'\left(\mathcal{R}\mathbf{u}_h\right), \mathcal{L}^*\mathbf{v}_h \right\rangle_K = L\left(\mathbf{v}_h\right). \tag{4.10}$$

From this point onwards, it only remains to choose a proper projection of the residual. A typical choice of the sub-grid scale space is the identity $P' = I$, leading to the Algebraic Sub-Grid Scale (ASGS) formulation, which means $\mathbf{v}'^{\perp} = \mathbf{0}$. Choosing $P' = I - P_h := P_h^{\perp}$, where $P_h$ is the $L^2$ projection onto the FE space (including boundary conditions) yields the Orthogonal Sub-Grid Scale (OSGS) formulation, because it corresponds to taking $\mathcal{X}'$ as the orthogonal complement of $\mathcal{X}_h$.

### *4.2 Sub-grid scales in the element edges*

The common procedure for the VMS formulation is to neglect the contribution of the sub-grid scales to the inter-element boundaries; however, enhanced stability properties can be achieved by considering them [35]. With the approach we follow, it is important to note that the sub-grid scales in the element interiors do not account for the boundary values, and the sub-grid scales in the inter-element boundaries have to be computed afterwards.

Let $\mathcal{E}_h = \{E\}$ the collection of interior edges of the FE partition, and $\mathbf{u}'_E$ the sub-grid scale on edge $E$,

assumed to be uniquely valued. The sub-grid scales on the edges of the boundary of $\Omega$ are taken as zero. Then, we may write equation (4.5) as:

$$B\left(\mathbf{u}_h, \mathbf{v}_h\right) + \sum_K \left\langle \mathbf{u}', \mathcal{L}^* \mathbf{v}_h \right\rangle_K + \sum_E \left\langle \mathbf{u}'_E, [\![ \mathcal{F}^* \mathbf{v}_h ]\!] \right\rangle_E = L(\mathbf{v}_h). \tag{4.11}$$

where $[\![ \mathcal{F}^* \mathbf{v}_h ]\!]$ denotes the jump of $\mathcal{F}^* \mathbf{v}_h$ across $E$, i.e., the sum of the values of $\mathcal{F}^* \mathbf{v}_h$ computed with the normals exterior to the elements that share edge $E$.

Imposing that the total fluxes are continuous across inter-element boundaries, it is argued in [36] that the sub-grid scales on the edges of the FE partition can be approximated by

$$\mathbf{u}'_E \approx -\frac{\delta}{2} [\![ \mathcal{F} \mathbf{u}_h ]\!],$$

where $\delta = \delta_0 h$ and $\delta_0$ is a dimensionless algorithmic parameter. Combining this with (4.9) we obtain the stabilized FE formulation:

$$B\left(\mathbf{u}_h, \mathbf{v}_h\right) + \sum_K \left\langle \boldsymbol{\tau}_K P'\left(\mathcal{R}\mathbf{u}_h\right), \mathcal{L}^* \mathbf{v}_h \right\rangle_K - \sum_E \frac{\delta}{2} \langle [\![ \mathcal{F} \mathbf{u}_h ]\!], [\![ \mathcal{F}^* \mathbf{v}_h ]\!] \rangle_E = L\left(\mathbf{v}_h\right). \tag{4.12}$$

## 5 Implementation

In this subsection, the stabilized formulation of the Reissner-Mindlin plate and the Timoshenko beam theories are presented. To simplify the exposition, in this section we consider only linear elements, and thus higher order derivatives in the element interiors are not considered. Nevertheless, the case of arbitrary order of interpolation will be analyzed in the following section.

Let us first write the Galerkin FE form of each problem:

- Reissner-Mindlin plate

$$k_1 \left(\nabla \boldsymbol{\theta}_h, \nabla \boldsymbol{\phi}_h\right) + k_2 \left(\nabla \cdot \boldsymbol{\theta}_h, \nabla \cdot \boldsymbol{\phi}_h\right) + \frac{1}{\varepsilon} \left(\nabla w_h - \boldsymbol{\theta}_h, \nabla v_h - \boldsymbol{\phi}_h\right) = \left\langle \mathbf{m}, \boldsymbol{\phi}_h \right\rangle + \left\langle q, v_h \right\rangle. \tag{5.1}$$

- Timoshenko beam

$$EI \left(\frac{d\theta_h}{dx}, \frac{d\phi_h}{dx}\right) + GA^* \left(\frac{dw_h}{dx} - \theta_h, \frac{dv_h}{dx} - \phi_h\right) = \left\langle m,\ \phi_h \right\rangle + \left\langle q,\ v_h \right\rangle. \tag{5.2}$$

Consider $\alpha$ and $\beta$ as the constants that multiply the shear and bending terms, respectively, namely $\alpha = GA^*$ and $\beta = EI$ for beams and $\alpha = \varepsilon^{-1}$, $\beta = Et^3/24$ for plates. In a general manner, the formulation yields a system of equations of the form

$$\begin{bmatrix} \alpha S_1 & \alpha S_2 \\ \alpha S_3 & \alpha S_4 + \beta B \end{bmatrix} \begin{bmatrix} W \\ \Theta \end{bmatrix} = \begin{bmatrix} F \\ M \end{bmatrix}, \tag{5.3}$$

where $W$ and $\Theta$ are the displacements and rotations arrays, respectively, $F$ is the array coming from the transverse loads, $M$ from the bending moments, $B$ and $S_i$ $(i = 1, 2, 3, 4)$ are the components arising from

the bending and shear terms, respectively (with $S_3 = S_2^T$). These notations can refer to matrix arrays depending on the problem. The standard formulations gives a symmetric system that locks when $t \to 0$ and $S_i \gg B$ (the inequality being understood component-wise), while in the stabilized formulations presented below, the stabilization terms allow the system to avoid the dominance of one term over the other.

In the following, the stabilization matrices are taken to be diagonal, of the form $\boldsymbol{\tau}_K = \mathrm{diag}(\tau_\theta, \tau_\theta, \tau_w)$ for plates and $\boldsymbol{\tau}_K = \mathrm{diag}(\tau_\theta, \tau_w)$ for beams, where $\tau_\theta$ and $\tau_w$ are still to be defined. It is understood that these parameters are evaluated element by element.

We will start writing the stabilized formulations without sub-grid scales on the inter-element boundaries. These will be introduced later, as they are the same for both the ASGS and the OSGS formulations.

### *5.1 Algebraic Sub-Grid Scales*

We first consider the ASGS formulation, which corresponds to $\mathbf{v}'^{\perp} = \mathbf{0}$. Then $P'$ is the identity on the element residuals, and thus $\mathbf{u}' = \boldsymbol{\tau}_K[\mathbf{f} - \mathcal{L}\mathbf{u}_h]$ in each element $K$. The formulation for linear elements and assuming constant stabilization parameters (i.e., constant element sizes) reads:

- Reissner-Mindlin plates:

$$\begin{aligned} &k_1 \left(\nabla \boldsymbol{\theta}_h, \nabla \boldsymbol{\phi}_h\right) + k_2 \left(\nabla \cdot \boldsymbol{\theta}_h, \nabla \cdot \boldsymbol{\phi}_h\right) + \frac{1}{\varepsilon} \left(\nabla w_h - \boldsymbol{\theta}_h, \nabla v_h - \boldsymbol{\phi}_h\right) \\ &\quad - \frac{\tau_w}{\varepsilon^2} \sum_K \langle \nabla \cdot \boldsymbol{\theta}_h, \nabla \cdot \boldsymbol{\phi}_h \rangle_K - \frac{\tau_\theta}{\varepsilon^2} \sum_K \langle \nabla w_h - \boldsymbol{\theta}_h, \nabla v_h - \boldsymbol{\phi}_h \rangle_K = \langle \mathbf{m}, \boldsymbol{\phi}_h \rangle + \langle q, v_h \rangle . \end{aligned} \tag{5.4}$$

- Timoshenko beams:

$$\begin{aligned} &EI \left( \frac{d\theta_h}{dx}, \frac{d\phi_h}{dx} \right) + GA^* \left( \frac{dw_h}{dx} - \theta_h, \frac{dv_h}{dx} - \phi_h \right) \\ &- \tau_w \left(GA^*\right)^2 \sum_K \left\langle \frac{d\theta_h}{dx} \, , \, \frac{d\phi_h}{dx} \right\rangle_K - \tau_\theta \left(GA^*\right)^2 \sum_K \left\langle \frac{dw_h}{dx} - \theta_h \, , \, \frac{dv_h}{dx} - \phi_h \right\rangle_K = \left\langle m, \, \phi_h \right\rangle + \left\langle q, \, v_h \right\rangle . \end{aligned} \tag{5.5}$$

In a general manner, the matrix version of these equations is

$$\begin{bmatrix} (\alpha - \tau_\theta \alpha^2) S_1 & (\alpha - \tau_\theta \alpha^2) S_2 \\ (\alpha - \tau_\theta \alpha^2) S_3 & (\alpha - \tau_\theta \alpha^2) S_4 + (\beta - \tau_w \alpha^2) B \end{bmatrix} \begin{bmatrix} W \\ \Theta \end{bmatrix} = \begin{bmatrix} F \\ M \end{bmatrix} . \tag{5.6}$$

This allows the system not to fall into shear dominance when $\boldsymbol{\tau}_K$ is properly designed. This part is crucial to obtain a locking-free formulation, and it will be explained below in more detail.

### *5.2 Orthogonal Sub-Grid Scales*

For this approach, the sub-grid scales are computed considering the orthogonal component of the residual as $\mathbf{u}' = \boldsymbol{\tau}_K P^{\perp}[\mathbf{f} - \mathcal{L}\mathbf{u}_h]$ in each element $K$, i.e., $P' = P^{\perp} = I - P_h$. If we denote, in a general manner, $\boldsymbol{\xi}_h = [\boldsymbol{\xi}_\theta, \xi_w]$ to be the FE projections of the residual onto $\mathcal{X}_h$, and $\boldsymbol{\eta}_h = [\boldsymbol{\eta}_\theta, \eta_w]$ to be the respective test functions in $\mathcal{X}_h$, the formulations for plates and beams can be written as:

- Reissner-Mindlin plates:

$$
\begin{aligned}
&k_1\left(\nabla\boldsymbol{\theta}_h,\nabla\boldsymbol{\phi}_h\right)+k_2\left(\nabla\cdot\boldsymbol{\theta}_h,\nabla\cdot\boldsymbol{\phi}_h\right)+\frac{1}{\varepsilon}\left(\nabla w_h-\boldsymbol{\theta}_h,\nabla v_h-\boldsymbol{\phi}_h\right)\\
&\quad-\frac{\tau_w}{\varepsilon^2}\sum_K\langle\nabla\cdot\boldsymbol{\theta}_h,\nabla\cdot\boldsymbol{\phi}_h\rangle_K-\frac{\tau_\theta}{\varepsilon^2}\sum_K\langle\nabla w_h-\boldsymbol{\theta}_h,\nabla v_h-\boldsymbol{\phi}_h\rangle_K\\
&\qquad+\frac{\tau_w}{\varepsilon}\sum_K\langle\xi_w,\nabla\cdot\boldsymbol{\phi}_h\rangle_K+\frac{\tau_\theta}{\varepsilon}\sum_K\langle\boldsymbol{\xi}_\theta,\nabla v_h-\boldsymbol{\phi}_h\rangle_K=\langle\mathbf{m},\boldsymbol{\phi}_h\rangle+\langle q,v_h\rangle,
\end{aligned}
\tag{5.7}
$$

$$
\frac{1}{\varepsilon}\left(\nabla\cdot\boldsymbol{\theta},\eta_w\right)-\left(\xi_w,\eta_w\right)=0,
\tag{5.8}
$$

$$
\frac{1}{\varepsilon}\left(\nabla w_h-\boldsymbol{\theta}_h,\boldsymbol{\eta}_\theta\right)-\left(\boldsymbol{\xi}_\theta,\boldsymbol{\eta}_\theta\right)=0,
\tag{5.9}
$$

for all $[\boldsymbol{\phi}_h, v_h] \in \mathcal{X}_h$ and $[\boldsymbol{\eta}_\theta, \eta_w] \in \mathcal{X}_h$.

- Timoshenko beams:

$$
\begin{aligned}
&EI\left(\frac{d\theta_h}{dx},\frac{d\phi_h}{dx}\right)+GA^*\left(\frac{dw_h}{dx}-\theta_h,\frac{dv_h}{dx}-\phi_h\right)\\
&-\tau_w(GA^*)^2\sum_K\left\langle\frac{d\theta_h}{dx}\,,\,\frac{d\phi_h}{dx}\right\rangle_K-\tau_\theta(GA^*)^2\sum_K\left\langle\frac{dw_h}{dx}-\theta_h\,,\,\frac{dv_h}{dx}-\phi_h\right\rangle_K\\
&\quad+\tau_wGA^*\sum_K\left\langle\xi_w\,,\,\frac{d\phi_h}{dx}\right\rangle_K+\tau_\theta GA^*\sum_K\left\langle\xi_\theta\,,\,\frac{dv_h}{dx}-\phi_h\right\rangle_K=\left\langle m,\,\phi_h\right\rangle+\left\langle q,\,v_h\right\rangle,
\end{aligned}
\tag{5.10}
$$

$$
GA^*\left(\frac{dw_h}{dx}-\theta_h\,,\,\eta_\theta\right)-\left(\xi_\theta\,,\,\eta_\theta\right)=0,
\tag{5.11}
$$

$$
GA^*\left(\frac{d\theta_h}{dx}\,,\,\eta_w\right)-\left(\xi_w\,,\,\eta_w\right)=0,
\tag{5.12}
$$

for all $[\phi_h, v_h] \in \mathcal{X}_h$ and $[\eta_\theta, \eta_w] \in \mathcal{X}_h$.

For this formulation, the matrix version of the equations is:

$$
\begin{bmatrix}
(\alpha-\tau_\theta\alpha^2)S_1 & (\alpha-\tau_\theta\alpha^2)S_2 & \tau_\theta\alpha P_1^\theta & 0\\
(\alpha-\tau_\theta\alpha^2)S_3 & (\alpha-\tau_\theta\alpha^2)S_4+(\beta-\tau_w\alpha^2)B & \tau_\theta\alpha P_2^\theta & \tau_w\alpha P^w\\
\alpha Q_1^\theta & \alpha Q_2^\theta & N & 0\\
0 & \alpha Q^w & 0 & N
\end{bmatrix}
\begin{bmatrix} W\\ \Theta\\ \Xi_\theta\\ \Xi_w \end{bmatrix}=
\begin{bmatrix} F\\ M\\ 0\\ 0 \end{bmatrix},
\tag{5.13}
$$

where $N$ is the Gram matrix, $P^w$ and $P_i^\theta$ $(i = 1, 2)$ are the matrices containing $\xi_w$ and $\xi_\theta$, respectively, with the corresponding test function associated to the index. In the same manner, $Q^w$ and $Q_i^\theta$ $(i = 1, 2)$ are the matrices containing deflection and rotations terms, depending on the index, with the test functions of the projection equations. Note that the system can be symmetrized by multiplying the last two rows by $\tau_\theta$ and $\tau_w$, respectively, since $(Q_i^\theta)^T = P_i^\theta$, $i = 1, 2$.

The OSGS implementation yields a system that shares some similarities with the mixed form of the problem. The difference is that the later yields a saddle point problem that is usually addressed using a mixed interpolation of the unknowns [10]. Note that similar formulations have been obtained in [4, 7, 11],

where the shear force is computed using the $L^2$ projection of the rotation onto the FE space in order to soothe the zero shear strain constraint of the problem, which differs from the sub-grid scale approach of the present work.

The implementation given by Eq. (5.13) is useful for the presentation of the formulation, but in practice two other alternatives are possible eliminating the degrees of freedom of the projections. One is an iterative deffect-correction approach, evaluating these projections at the previous iteration when computing displacements and rotations and then updating them. The other is a condensation of the projections, which implies an increase of the stencil of the stiffness matrix. Both approaches are feasible because the matrix that multiplies the degrees of freedom of the rotations is a mass matrix, easily invertible (in a direct or in an iterative way). In this case, the formulation presented should be compared to those that do not introduce new variables, but solve only for displacements and rotations.

### *5.3 Inter-element edge stabilization*

The stabilization using the sub-grid scales in the element edges can be implemented independently of the sub-grid scales in the element interiors, as stated in section 4. For the implementation, consider the terms from the sub-grid scale in the inter-element edges added to the Galerkin form of the problem. The resulting discrete problem is:

- Reissner-Mindlin plate

$$\begin{aligned} k_1\left(\nabla\boldsymbol{\theta}_h,\nabla\boldsymbol{\phi}_h\right)+k_2\left(\nabla\cdot\boldsymbol{\theta}_h,\nabla\cdot\boldsymbol{\phi}_h\right)+\frac{1}{\varepsilon}\left(\nabla w_h-\boldsymbol{\theta}_h,\nabla v_h-\boldsymbol{\phi}_h\right)\\ -\frac{\delta k_1}{2}\sum_E\langle[\![\mathbf{n}\cdot\nabla\boldsymbol{\theta}_h]\!],[\![\mathbf{n}\cdot\nabla\boldsymbol{\phi}_h]\!]\rangle_E-\frac{\delta k_2}{2}\sum_E\langle[\![\mathbf{n}\nabla\cdot\boldsymbol{\theta}_h]\!],[\![\mathbf{n}\nabla\cdot\boldsymbol{\phi}_h]\!]\rangle_E\\ -\frac{\delta}{2\varepsilon}\sum_E\langle[\![\mathbf{n}\cdot\nabla w_h]\!],[\![\mathbf{n}\cdot\nabla v_h]\!]\rangle_E=\langle\mathbf{m},\boldsymbol{\phi}_h\rangle+\langle q,v_h\rangle. \end{aligned} \tag{5.14}$$

- Timoshenko beam

$$\begin{aligned} EI\left(\frac{d\theta_h}{dx},\frac{d\phi_h}{dx}\right)+GA^*\left(\frac{dw_h}{dx}-\theta_h,\frac{dv_h}{dx}-\phi_h\right)\\ -\frac{\delta EI}{2}\sum_E\left\langle\left[\!\left[\frac{d\theta_h}{dx}\right]\!\right],\left[\!\left[\frac{d\phi_h}{dx}\right]\!\right]\right\rangle_E-\frac{\delta GA^*}{2}\sum_E\left\langle\left[\!\left[\frac{dw_h}{dx}\right]\!\right],\left[\!\left[\frac{dv_h}{dx}\right]\!\right]\right\rangle_E=\left\langle m,\ \phi_h\right\rangle+\left\langle q,\ v_h\right\rangle. \end{aligned} \tag{5.15}$$

Recall that, in both problems, $\delta$ is a parameter of the order of the element size.

### *5.4 Stabilization parameters*

The design of $\boldsymbol{\tau}_K$ is based on the definition proposed in [37] for the Reissner-Mindlin case, with some modifications. According to that work, shear dominance can be dealt with by just introducing the shear stabilization parameter $\tau_\theta$, and it was successful in that regard. However, convergence ratios were not tested. Taking this into consideration, the stabilization parameters are defined as

- Reissner-Mindlin plate:

$$\boldsymbol{\tau}_K = \operatorname{diag}(\tau_\theta, \tau_\theta, \tau_w), \qquad \tau_\theta = \left(c_1 \frac{k}{h^2} + c_2 \varepsilon^{-1}\right)^{-1}, \qquad \tau_w = \left(c_3 \frac{\varepsilon^{-1}}{h^2} + c_4 \frac{\varepsilon^{-2}}{k}\right)^{-1}, \tag{5.16}$$

- Timoshenko beam:

$$\boldsymbol{\tau}_K = \operatorname{diag}(\tau_\theta, \tau_w), \qquad \tau_\theta = \left(c_1 \frac{EI}{h^2} + c_2 GA^*\right)^{-1}, \qquad \tau_w = \left(c_3 \frac{GA^*}{h^2} + c_4 \frac{(GA^*)^2}{EI}\right)^{-1}, \tag{5.17}$$

where $h$ is the element size, $k = k_1 + k_2$, and $c_i$, $i = 1, 2$ are constants to be defined. Note that in [37] the constant $c_2$ must be taken as $c_2 = 1$ to eliminate shear dominance; this is confirmed in the stability analysis in section 6. In [31] the ASGS formulation is used together with the DSG approach taking $\tau_w = 0$ and a similar expression of $\tau_\theta$ to the one we propose, but taking also into account the possible anisotropy of the elements.

To find which values of the stabilization constants can be used in the stabilization parameters, the matrix form of the equations using the ASGS formulation of (5.6) is compared to the exact solution of the elastic equations for the bending of an unloaded beam using Timoshenko's theory. Consider a two noded beam of length $L$, with nodal deflections $w_i$ and rotations $\theta_i$, for nodes $i = 1, 2$, and the corresponding nodal loads $P_i$ and $M_i$. For $\mu = \frac{12EI}{GA^*L^2}$, the following system of equations is obtained:

$$\begin{bmatrix} \frac{12EI}{(1+\mu)L^3} & \frac{6EI}{(1+\mu)L^2} & -\frac{12EI}{(1+\mu)L^3} & \frac{6EI}{(1+\mu)L^2} \\ \frac{6EI}{(1+\mu)L^2} & \frac{(4+\mu)EI}{(1+\mu)L} & -\frac{12EI}{(1+\mu)L^2} & \frac{(2-\mu)EI}{(1+\mu)L} \\ -\frac{12EI}{(1+\mu)L^2} & -\frac{6EI}{(1+\mu)L^2} & \frac{12EI}{(1+\mu)L^2} & -\frac{6EI}{(1+\mu)L^2} \\ \frac{6EI}{(1+\mu)L^2} & \frac{(2-\mu)EI}{(1+\mu)L} & -\frac{12EI}{(1+\mu)L^2} & \frac{(4+\mu)EI}{(1+\mu)L} \end{bmatrix} \begin{bmatrix} w_1 \\ \theta_1 \\ w_2 \\ \theta_2 \end{bmatrix} = \begin{bmatrix} P_1 \\ M_1 \\ P_2 \\ M_2 \end{bmatrix}. \tag{5.18}$$

Comparing this system to the one obtained using the stabilized FE approximation we propose, we obtain that, in the ASGS formulation of beams, the stabilization constants can be taken as $c_1 = c_3 = 12$ and $c_2 = c_4 = 1$. In this case, the stiffness matrix of an element of length $L$ is exactly the same as that of the elastic equations of a Timoshenko beam. The behavior of the FE formulation in response to this selection of constants as well as the constants used in the OSGS formulation will be discussed in section 7.

## 6 Numerical Analysis

In this section, the numerical analysis of the stabilized formulation for plates is analysed. The results are inherited by the beam problem since it is equivalent to the dimensional reduction of the plate problem.

Consider $\|\cdot\|$ to be the $L^2(\Omega)$ norm. Let us define some inequalities that will allow us to obtain a stability estimate. For simplicity, we will assume the FE partition to be quasi-uniform, of size $h$. We may thus assume that there is a constant $C_{\text{inv}}$, independent of the mesh size $h$, such that the following inverse estimate holds:

$$\|\nabla v_h\|_K \leqslant \frac{C_{\text{inv}}}{h} \|v_h\|_K, \tag{6.1}$$

for all FE functions $v_h$ defined on the partition $\{K\}$. Similarly, the following trace inequality holds: there exists a a constant $C_{\text{trace}}$ independent of $h$ such that

$$\|v\|_{\partial K}^2 \leqslant C_{\text{trace}} \left( \frac{1}{h} \|v\|_K^2 + h \|\nabla v\|_K^2 \right), \tag{6.2}$$

for functions $v \in H^1(K)$. In this expression, the last term is dropped if $v$ is a polynomial on the element domain $K$.

Let now $\mathcal{E}_h = \{E\}$ be the edges of the FE partition. For piecewise discontinuous polynomials $\varphi_h$ and continuous polynomials $\psi_h$ there holds:

$$\sum_E \| [\![ \boldsymbol{n} \varphi_h ]\!] \|_E^2 \leqslant 2 \frac{C_{\text{trace}}}{h} \sum_K \|\varphi_h\|_K^2, \qquad \sum_E \|\psi_h\|_E^2 \leqslant \frac{C_{\text{trace}}}{2h} \sum_K \|\psi_h\|_K^2. \tag{6.3}$$

In the following, $C$ will denote a generic positive constant, not necessarily the same at different occurrences.

The stabilized FE formulation for elements of arbitrary polynomial degree can be written as:

$$B_{\text{stab}}(\mathbf{u}_h, \mathbf{v}_h) = L_{\text{stab}}(\mathbf{v}_h), \tag{6.4}$$

where

$$\begin{aligned} B_{\text{stab}}(\mathbf{u}_h, \mathbf{v}_h) = {} & k_1 \left( \nabla \boldsymbol{\theta}_h, \nabla \boldsymbol{\phi}_h \right) + k_2 \left( \nabla \cdot \boldsymbol{\theta}_h, \nabla \cdot \boldsymbol{\phi}_h \right) + \frac{1}{\varepsilon} \left( \nabla w_h - \boldsymbol{\theta}_h, \nabla v_h - \boldsymbol{\phi}_h \right) \\ & + \tau_\theta \sum_K \left\langle P' \left[ k_1 \Delta \boldsymbol{\theta}_h + k_2 \nabla (\nabla \cdot \boldsymbol{\theta}_h) + \frac{1}{\varepsilon} \left( \nabla w_h - \boldsymbol{\theta}_h \right) \right], -k_1 \Delta \boldsymbol{\phi}_h - k_2 \nabla (\nabla \cdot \boldsymbol{\phi}_h) - \frac{1}{\varepsilon} \left( \nabla v_h - \boldsymbol{\phi}_h \right) \right\rangle_K \\ & + \tau_w \sum_K \left\langle P' \left[ \frac{1}{\varepsilon} \nabla \cdot \left( \nabla w_h - \boldsymbol{\theta}_h \right) \right], -\frac{1}{\varepsilon} \nabla \cdot \left( \nabla v_h - \boldsymbol{\phi}_h \right) \right\rangle_K, \end{aligned} \tag{6.5}$$

and

$$\begin{aligned} L_{\text{stab}}(\mathbf{v}_h) = {} & \langle \mathbf{m}, \boldsymbol{\phi}_h \rangle + \langle q, v_h \rangle - \tau_\theta \sum_K \left\langle P' \left[ \mathbf{m} \right], -k_1 \Delta \boldsymbol{\phi}_h - k_2 \nabla (\nabla \cdot \boldsymbol{\phi}_h) - \frac{1}{\varepsilon} \left( \nabla v_h - \boldsymbol{\phi}_h \right) \right\rangle_K \\ & - \tau_w \sum_K \left\langle P' \left[ q \right], -\frac{1}{\varepsilon} \nabla \cdot \left( \nabla v_h - \boldsymbol{\phi}_h \right) \right\rangle_K, \end{aligned} \tag{6.6}$$

where $P' = I$ for the ASGS formulation and $P' = P^\perp$ for the OSGS method.

### *6.1 Stability analysis of the Algebraic Sub-Grid Scale formulation*

Let us first recall the stability estimate presented in [37] for the plate problem, where the ASGS approach was considered. In that work the terms multiplied by $\tau_w$ were neglected because they were not needed to get rid of the numerical locking. This fact however, does not account for the convergence rate of the solution, and $\tau_w$ is indeed necessary for it to be optimal, as will be explained and numerically proven below. The formulation analyzed in [37] will now be extended in the same manner: for the stability estimate, take

$\mathbf{v}_h = \mathbf{u}_h$ and consider $\boldsymbol{\gamma}_h = \nabla w_h - \boldsymbol{\theta}_h$. Using Schwarz's inequality leads to:

$$B_{\text{stab}}(\mathbf{u}_h, \mathbf{u}_h) \geqslant \sum_K \Big[ k_1 \|\nabla \boldsymbol{\theta}_h\|_K^2 + k_2 \|\nabla \cdot \boldsymbol{\theta}_h\|_K^2 + \frac{1}{\varepsilon} \|\boldsymbol{\gamma}_h\|_K^2 - \tau_\theta k_1^2 \|\Delta \boldsymbol{\theta}_h\|_K^2 - \tau_\theta k_2^2 \|\nabla (\nabla \cdot \boldsymbol{\theta}_h)\|_K^2 - \tau_\theta \frac{1}{\varepsilon^2} \|\boldsymbol{\gamma}_h\|_K^2$$
$$- 2\tau_\theta \frac{k_1}{\varepsilon} \|\Delta \boldsymbol{\theta}_h\|_K \|\boldsymbol{\gamma}_h\|_K - 2\tau_\theta \frac{k_2}{\varepsilon} \|\nabla (\nabla \cdot \boldsymbol{\theta}_h)\|_K \|\boldsymbol{\gamma}_h\|_K - 2\tau_\theta k_1 k_2 \|\Delta \boldsymbol{\theta}_h\|_K \|\nabla (\nabla \cdot \boldsymbol{\theta}_h)\|_K - \tau_w \frac{1}{\varepsilon^2} \|\nabla \cdot \boldsymbol{\gamma}_h\|_K^2 \Big]. \tag{6.7}$$

Using the inverse estimate (6.1) and Young's inequality, we obtain:

$$\begin{aligned} B_{\text{stab}}(\mathbf{u}_h, \mathbf{u}_h) \geqslant & \sum_K \Big[ k_1 \|\nabla \boldsymbol{\theta}_h\|_K^2 + k_2 \|\nabla \cdot \boldsymbol{\theta}_h\|_K^2 + \frac{1}{\varepsilon} \|\boldsymbol{\gamma}_h\|_K^2 - \tau_\theta k_1^2 \frac{C_{\text{inv}}^2}{h^2} \|\nabla \boldsymbol{\theta}_h\|_K^2 - \tau_\theta k_2^2 \frac{C_{\text{inv}}^2}{h^2} \|\nabla \cdot \boldsymbol{\theta}_h\|_K^2 - \tau_\theta \frac{1}{\varepsilon^2} \|\boldsymbol{\gamma}_h\|_K^2 \\ & - \tau_\theta \frac{k_1}{\varepsilon} \left( \|\nabla \boldsymbol{\theta}_h\|_K^2 + \frac{C_{\text{inv}}^2}{h^2} \|\boldsymbol{\gamma}_h\|_K^2 \right) - \tau_\theta \frac{k_2}{\varepsilon} \left( \|\nabla \cdot \boldsymbol{\theta}_h\|_K^2 + \frac{C_{\text{inv}}^2}{h^2} \|\boldsymbol{\gamma}_h\|_K^2 \right) \\ & - \tau_\theta \left( k_1^2 \frac{C_{\text{inv}}^2}{h^2} \|\nabla \boldsymbol{\theta}_h\|_K^2 + k_2^2 \frac{C_{\text{inv}}^2}{h^2} \|\nabla \cdot \boldsymbol{\theta}_h\|_K^2 \right) - \tau_w \frac{1}{\varepsilon^2} \frac{C_{\text{inv}}^2}{h^2} \|\boldsymbol{\gamma}_h\|_K^2 \Big] \\ = & \sum_K \Big[ \beta_1 \|\nabla \boldsymbol{\theta}_h\|_K^2 + \beta_2 \|\nabla \cdot \boldsymbol{\theta}_h\|_K^2 + \beta_3 \|\boldsymbol{\gamma}_h\|_K^2 \Big], \end{aligned} \tag{6.8}$$

where

$$\beta_1 = \tau_\theta \left[ c_1 \frac{k_1^2}{h^2} + c_1 \frac{k_1 k_2}{h^2} + c_2 \frac{k_1}{\varepsilon} - 2 \frac{C_{\text{inv}}^2}{h^2} k_1^2 - \frac{k_1}{\varepsilon} \right], \tag{6.9}$$

$$\beta_2 = \tau_\theta \left[ c_1 \frac{k_1 k_2}{h^2} + c_1 \frac{k_2^2}{h^2} + c_2 \frac{k_2}{\varepsilon} - 2 \frac{C_{\text{inv}}^2}{h^2} k_2^2 - \frac{k_2}{\varepsilon} \right], \tag{6.10}$$

$$\beta_3 = \tau_\theta \left[ c_1 \frac{k}{h^2 \varepsilon} + c_2 \frac{1}{\varepsilon^2} - \frac{1}{\varepsilon^2} - \frac{k}{\varepsilon} \frac{C_{\text{inv}}^2}{h^2} - \frac{k}{\varepsilon} \frac{C_{\text{inv}}^2}{h^2} \left( \frac{c_1 k \varepsilon + c_2 h^2}{c_3 k \varepsilon + c_4 h^2} \right) \right]. \tag{6.11}$$

Estimate (6.8) is not satisfactory because it does not provide a proper balance of the powers of the thickness in the different terms it involves. This occurs regardless of the selection of stabilization parameters, with the only exception of $c_1 = c_3 = 12$, and $c_2 = c_4 = 1$, which allow one to recover the stiffness matrix coming from the elastic equations (5.18). To understand the reason, suppose that the physical properties and the mesh size $h$ are fixed and let us analyze the scaling of the parameters $\beta_i$, $i = 1, 2, 3$, with respect to the thickness $t$. Assuming $c_3 \geqslant c_1$, $c_4 \geqslant c_2$ and $c_1 > 2C_{\text{inv}}^2$ and noting that $k_1$, $k_2$ scale as $t^3$ and $\varepsilon$ scales as $t^{-1}$, we have that

$$\beta_1, \beta_2 \sim \tau_\theta t^4 \left[ A_1 \frac{t^2}{h^2} + A_2 (c_2 - 1) \right], \qquad \beta_3 \sim \tau_\theta t^4 \left[ B_1 \frac{1}{h^2} + \frac{B_2}{t^2} (c_2 - 1) \right], \tag{6.12}$$

where $\sim$ stands for scaling and $A_1$, $A_2$, $B_1$, $B_2$ are independent of $t$ and $h$. From this we observe that in order to avoid shear locking we need to take $c_2 = 1$, as it was observed in [37], but in this case also the last term in $\beta_1$, $\beta_2$ vanishes, and we have that $\beta_1$, $\beta_2 = \mathcal{O}(\tau_\theta t^6)$ while $\beta_3 = \mathcal{O}(\tau_\theta t^4)$ (for $h$ fixed). Therefore, the stability estimate (6.8) does not provide a balanced control of the shear term and the derivatives of the rotation when $t \to 0$. We will see in the next subsection that the OSGS formulation does not suffer from this misbehavior.

### *6.2 Stability and convergence analysis of the Orthogonal Sub-Grid Scale formulation*

The numerical analysis of the method considering the OSGS approach is presented next. For positive and dimensionally correct $\alpha_i$ $(i = 1, 2, 3)$, the norm in which the results are presented is:

$$|||\mathbf{v}_h|||^2 := \alpha_1 \|\nabla \boldsymbol{\phi}_h\|^2 + \alpha_2 \|\nabla \cdot \boldsymbol{\phi}_h\|^2 + \alpha_3 \|\boldsymbol{\gamma}_h\|^2 . \tag{6.13}$$

This norm has the same form as for the Galerkin method and the ASGS formulation (see estimate (6.8)), but with the advantage that the constants $\alpha_i$ are such that locking is no longer possible, because they are designed in a manner that none of them can become dominant over the others. In particular, it will be shown that they behave as $\alpha_1,\ \alpha_2 = \mathcal{O}(\tau_\theta t^4)$ and $\alpha_3 = \mathcal{O}(\tau_\theta t^4 h^{-2})$.

In the following, it will be proved that the formulation is stable under the norm (6.13), in the form of the inf-sup condition.

**Theorem 6.1 (Stability).** *There is a constant $C > 0$ such that*

$$\inf_{\mathbf{u}_h \in \mathcal{X}_h} \sup_{\mathbf{v}_h \in \mathcal{X}_h} \frac{B_{\text{stab}}(\mathbf{u}_h, \mathbf{v}_h)}{|||\mathbf{u}_h||| \, |||\mathbf{v}_h|||} \geqslant C. \tag{6.14}$$

*Proof.* Let us start noting that for any function $\mathbf{u}_h \in \mathcal{X}_h$ we have

$$\begin{aligned} B_{\text{stab}}(\mathbf{u}_h, \mathbf{u}_h) =& k_1 \|\nabla \boldsymbol{\theta}_h\|^2 + k_2 \|\nabla \cdot \boldsymbol{\theta}_h\|^2 + \varepsilon^{-1} \|\boldsymbol{\gamma}_h\|^2 \\ & - \tau_\theta \sum_K \left\| P^\perp \left( k_1 \Delta \boldsymbol{\theta}_h + k_2 \nabla(\nabla \cdot \boldsymbol{\theta}_h) + \varepsilon^{-1} \boldsymbol{\gamma}_h \right) \right\|_K^2 - \tau_w \sum_K \left\| P^\perp \left( \varepsilon^{-1} \nabla \cdot \boldsymbol{\gamma}_h \right) \right\|_K^2 . \end{aligned} \tag{6.15}$$

It is important to note that the Galerkin terms of the bilinear form $B$ have already the necessary terms to have control over the $\nabla \boldsymbol{\theta}_h$ and $\boldsymbol{\gamma}_h$. However, the problem arises when $t \to 0$ and becomes shear dominant. Because of this, the main idea is to obtain a stability estimate in which the shear dominance can be prevented. This estimate comes from the terms whose orthogonal projections appear in $B_{\text{stab}}$, which is obtained by bounding the bilinear form term by term as follows.

Let us consider $\mathbf{v}_{h1} := (\tau_\theta \boldsymbol{\phi}_1, 0)$, where $\boldsymbol{\phi}_1 = P_h \left( k_1 \Delta \boldsymbol{\theta}_h + k_2 \nabla(\nabla \cdot \boldsymbol{\theta}_h) + \varepsilon^{-1} \boldsymbol{\gamma}_h \right)$ and $P_h$ is the $L^2$ projection onto the FE space. It is understood that the term inside the projection is evaluated element-wise. Taking $\mathbf{v}_{h1}$ as test function in the bilinear form, and integrating by parts the Galerkin terms, yields

$$\begin{aligned} B_{\text{stab}}(\mathbf{u}_h, \mathbf{v}_{h1}) =& - \sum_K \tau_\theta \left\langle k_1 \Delta \boldsymbol{\theta}_h + k_2 \nabla(\nabla \cdot \boldsymbol{\theta}_h) + \varepsilon^{-1} \boldsymbol{\gamma}_h, \boldsymbol{\phi}_1 \right\rangle_K + \tau_\theta \sum_E \langle [\![ k_1 \mathbf{n} \cdot \nabla \boldsymbol{\theta}_h ]\!] + [\![ k_2 \mathbf{n} \nabla \cdot \boldsymbol{\theta}_h ]\!], \boldsymbol{\phi}_1 \rangle_E \\ & - \tau_\theta^2 \sum_K \left\langle P^\perp \left( k_1 \Delta \boldsymbol{\theta}_h + k_2 \nabla(\nabla \cdot \boldsymbol{\theta}_h) + \varepsilon^{-1} \boldsymbol{\gamma}_h \right), k_1 \Delta \boldsymbol{\phi}_1 + k_2 \nabla(\nabla \cdot \boldsymbol{\phi}_1) - \varepsilon^{-1} \boldsymbol{\phi}_1 \right\rangle_K \\ & - \tau_\theta \tau_w \sum_K \left\langle P^\perp \left( \varepsilon^{-1} \nabla \cdot \boldsymbol{\gamma}_h \right), -\varepsilon^{-1} \nabla \cdot \boldsymbol{\phi}_1 \right\rangle_K . \end{aligned} \tag{6.16}$$

Note that the equation contains terms projected in the space that is orthogonal to the FE space, which disappear when tested with $\boldsymbol{\phi}_1$ because it belongs to the FE space itself. Then, by using Schwarz's inequality and the inverse estimate (6.1), we obtain:

$$B_{\text{stab}}(\mathbf{u}_h, \mathbf{v}_{h1}) \geqslant - \tau_\theta \sum_K \|\boldsymbol{\phi}_1\|_K^2 - \tau_\theta \sum_E \|[\![ k_1 \mathbf{n} \cdot \nabla \boldsymbol{\theta}_h ]\!]\|_E \, \|\boldsymbol{\phi}_1\|_E - \tau_\theta \sum_E \|[\![ k_2 \mathbf{n} \nabla \cdot \boldsymbol{\theta}_h ]\!]\|_E \, \|\boldsymbol{\phi}_1\|_E$$

$$- \tau_\theta^2 k \frac{C_{\text{inv}}^2}{h^2} \sum_K \left\| P^\perp \left( k_1 \Delta \boldsymbol{\theta}_h + k_2 \nabla(\nabla \cdot \boldsymbol{\theta}_h) + \varepsilon^{-1} \boldsymbol{\gamma}_h \right) \right\|_K \left\| \boldsymbol{\phi}_1 \right\|_K$$
$$- \tau_\theta \tau_w \varepsilon^{-1} \frac{C_{\text{inv}}}{h} \sum_K \left\| P^\perp \left( \varepsilon^{-1} \nabla \cdot \boldsymbol{\gamma}_h \right) \right\|_K \left\| \boldsymbol{\phi}_1 \right\|_K . \tag{6.17}$$

Then, using Young's inequality and the trace inequalities (6.3) it follows that:

$$\begin{aligned} B_{\text{stab}}(\mathbf{u}_h, \mathbf{v}_{h1}) \geqslant & - \tau_\theta \sum_K \|\boldsymbol{\phi}_1\|_K^2 - \tau_\theta \sum_K \|\boldsymbol{\phi}_1\|_K^2 - \tau_\theta \frac{C_{\text{trace}}^2}{2h^2} \sum_K \|k_1 \nabla \boldsymbol{\theta}_h\|_K^2 - \tau_\theta \frac{C_{\text{trace}}^2}{2h^2} \sum_K \|k_2 \nabla \cdot \boldsymbol{\theta}_h\|_K^2 \\ & - \frac{\tau_\theta^2 k}{2} \frac{C_{\text{inv}}^2}{h^2} \sum_K \left( \|\boldsymbol{\phi}_1\|_K^2 + \left\| P^\perp \left( k_1 \Delta \boldsymbol{\theta}_h + k_2 \nabla(\nabla \cdot \boldsymbol{\theta}_h) + \varepsilon^{-1} \boldsymbol{\gamma}_h \right) \right\|_K^2 \right) \\ & - \tau_\theta \tau_w \frac{\varepsilon^{-1}}{2} \frac{C_{\text{inv}}^2}{h^2} \sum_K \|\boldsymbol{\phi}_1\|_K^2 - \tau_\theta \tau_w \frac{\varepsilon^{-1}}{2} \sum_K \left\| P^\perp \left( \varepsilon^{-1} \nabla \cdot \boldsymbol{\gamma}_h \right) \right\|_K^2 . \end{aligned} \tag{6.18}$$

Similarly, consider $\mathbf{v}_{h2} = (\mathbf{0}, \tau_w v_2)$, where $v_2 = P_h \left( \varepsilon^{-1} \nabla \cdot \boldsymbol{\gamma}_h \right)$, as test function in the bilinear form. We have that

$$\begin{aligned} B_{\text{stab}}(\mathbf{u}_h, \mathbf{v}_{h2}) = & - \tau_w \left( \varepsilon^{-1} \nabla \cdot \boldsymbol{\gamma}_h, v_2 \right) + \tau_w \sum_E \left\langle \varepsilon^{-1} \left[\!\left[ \mathbf{n} \cdot \boldsymbol{\gamma}_h \right]\!\right], v_2 \right\rangle_E \\ & - \tau_w^2 \varepsilon^{-1} \sum_K \left\langle P^\perp \left( \varepsilon^{-1} \nabla \cdot \boldsymbol{\gamma}_h \right), \nabla \cdot \nabla v_2 \right\rangle_K \\ & - \tau_\theta \tau_w \varepsilon^{-1} \sum_K \left\langle P^\perp \left( k_1 \Delta \boldsymbol{\theta}_h + k_2 \nabla(\nabla \cdot \boldsymbol{\theta}_h) + \varepsilon^{-1} \boldsymbol{\gamma}_h \right), \nabla v_2 \right\rangle_K . \end{aligned} \tag{6.19}$$

Then following the same procedure as before, it follows that

$$\begin{aligned} B_{\text{stab}}(\mathbf{u}_h, \mathbf{v}_{h2}) \geqslant & - \tau_w \sum_K \|v_2\|_K^2 - \tau_w \sum_K \|v_2\|_K^2 - \tau_w \frac{C_{\text{trace}}^2}{4h^2} \sum_K \left\| \varepsilon^{-1} \boldsymbol{\gamma}_h \right\|_K^2 \\ & - \tau_w^2 \frac{\varepsilon^{-1}}{2} \frac{C_{\text{inv}}^2}{h^2} \sum_K \left( \|v_2\|_K^2 + \left\| P^\perp \left( \varepsilon^{-1} \nabla \cdot \boldsymbol{\gamma}_h \right) \right\|_K^2 \right) \\ & - \tau_\theta \tau_w \frac{\varepsilon^{-1}}{2} \sum_K \|v_2\|_K^2 - \tau_\theta \tau_w \frac{\varepsilon^{-1}}{2} \frac{C_{\text{inv}}^2}{h^2} \sum_K \left\| P^\perp \left( k_1 \Delta \boldsymbol{\theta}_h + k_2 \nabla(\nabla \cdot \boldsymbol{\theta}_h) + \varepsilon^{-1} \boldsymbol{\gamma}_h \right) \right\|_K^2 . \end{aligned} \tag{6.20}$$

Lastly, consider $\mathbf{v}_h = \mathbf{u}_h + \frac{1}{2}\mathbf{v}_{h1} + \frac{1}{2}\mathbf{v}_{h2}$, which is equivalent to adding up (6.15), $\frac{1}{2}$(6.18), and $\frac{1}{2}$(6.20). This yields

$$\begin{aligned} B_{\text{stab}}(\mathbf{u}_h, \mathbf{v}_h) \geqslant & \left( k_1 - \tau_\theta k_1^2 \frac{C_{\text{trace}}^2}{4h^2} \right) \|\nabla \boldsymbol{\theta}_h\|^2 + \left( k_2 - \tau_\theta k_2^2 \frac{C_{\text{trace}}^2}{4h^2} \right) \|\nabla \cdot \boldsymbol{\theta}_h\|^2 + \left( \varepsilon^{-1} - \tau_w \varepsilon^{-2} \frac{C_{\text{trace}}^2}{8h^2} \right) \|\boldsymbol{\gamma}_h\|^2 \\ & - \left( \tau_\theta + \frac{\tau_\theta^2 k}{2} \frac{C_{\text{inv}}^2}{h^2} + \tau_\theta \tau_w \frac{\varepsilon^{-1}}{2} \frac{C_{\text{inv}}^2}{h^2} \right) \sum_K \left\| k_1 \Delta \boldsymbol{\theta}_h + k_2 \nabla(\nabla \cdot \boldsymbol{\theta}_h) + \varepsilon^{-1} \boldsymbol{\gamma}_h \right\|_K^2 \\ & - \left( \tau_w + \tau_\theta \tau_w \frac{\varepsilon^{-1}}{2} + \tau_w^2 \frac{\varepsilon^{-1}}{2} \frac{C_{\text{inv}}^2}{h^2} \right) \sum_K \left\| \varepsilon^{-1} \nabla \cdot \boldsymbol{\gamma}_h \right\|_K^2 . \end{aligned} \tag{6.21}$$

The last two terms can be separated using the triangular inequality, enabling us to write the expression in terms of the original variables only:

$$B_{\text{stab}}(\mathbf{u}_h, \mathbf{v}_h) \geqslant \alpha_1 \|\nabla \boldsymbol{\theta}_h\|^2 + \alpha_2 \|\nabla \cdot \boldsymbol{\theta}_h\|^2 + \alpha_3 \|\boldsymbol{\gamma}_h\|^2 \equiv |||\mathbf{u}_h|||^2, \tag{6.22}$$

where

$$\alpha_1 = \tau_\theta \left[ c_1 \frac{k k_1}{h^2} + c_2 \frac{k_1}{\varepsilon} - k_1^2 \frac{C_{\text{inv}}^2}{4h^2} \left( \frac{C_{\text{inv}} k\varepsilon}{c_1 k\varepsilon + c_2 h^2} \right) - k_1^2 \frac{C_{\text{inv}}^2}{4h^2} \left( \frac{C_{\text{inv}}^2 k\varepsilon}{c_3 k\varepsilon + c_4 h^2} \right) - k_1^2 \frac{C_{\text{trace}}^2}{4h^2} \right], \tag{6.23}$$

$$\alpha_2 = \tau_\theta \left[ c_1 \frac{k k_2}{h^2} + c_2 \frac{k_2}{\varepsilon} - k_2^2 \frac{C_{\text{inv}}^2}{4h^2} \left( \frac{C_{\text{inv}} k\varepsilon}{c_1 k\varepsilon + c_2 h^2} \right) - k_2^2 \frac{C_{\text{inv}}^2}{4h^2} \left( \frac{C_{\text{inv}}^2 k\varepsilon}{c_3 k\varepsilon + c_4 h^2} \right) - k_2^2 \frac{C_{\text{trace}}^2}{4h^2} \right], \tag{6.24}$$

$$\begin{aligned} \alpha_3 = \tau_\theta \Bigg[ & c_1 \frac{k\varepsilon^{-1}}{h^2} + \frac{c_2}{\varepsilon^2} - \frac{1}{\varepsilon^2} - \frac{k}{\varepsilon} \frac{C_{\text{inv}}^2}{4h^2} \left( \frac{h^2}{c_1 k\varepsilon + c_2 h^2} \right) - \frac{k}{\varepsilon} \frac{C_{\text{inv}}^2}{4h^2} \left( \frac{h^2}{c_3 k\varepsilon + c_4 h^2} \right) - \frac{k}{\varepsilon} \frac{C_{\text{trace}}^2}{8h^2} \left( \frac{c_1 k\varepsilon + c_2 h^2}{c_3 k\varepsilon + c_4 h^2} \right) \\ & - \frac{k}{\varepsilon} \frac{C_{\text{inv}}^2}{h^2} \left( \frac{c_1 k\varepsilon + c_2 h^2}{c_3 k\varepsilon + c_4 h^2} \right) - \frac{k}{\varepsilon} \frac{C_{\text{inv}}^2}{2h^2} \left( \frac{c_1 k\varepsilon + c_2 h^2}{c_3 k\varepsilon + c_4 h^2} \right) \left( \frac{C_{\text{inv}}^2 k\varepsilon^{-1}}{c_3 k\varepsilon^{-1} + c_4 \varepsilon^{-2} h^2} \right) \Bigg]. \end{aligned} \tag{6.25}$$

From the expression in (6.25) it can be verified again that the value $c_2 = 1$ is necessary to eliminate shear dominance and that the constants must satisfy $c_3 \geqslant c_1$ and $c_4 \geqslant c_2$. It is also needed that $c_1 > 2C_{\text{inv}}^2 + \frac{1}{4} C_{\text{trace}}^2$. In fact, for linear elements it suffices to take $c_1 > 0$, as the integration by parts in (6.16) is not needed (the terms multiplied by $C_{\text{trace}}$ do not show up) and one may take the constant associated to the inverse estimate for second derivatives as $C_{\text{inv}} = 0$. Under all these conditions, it is readily checked that

$$\alpha_1, \alpha_2 \sim \tau_\theta t^4 \left[ A_1' \frac{t^2}{h^2} + A_2' c_2 \right], \qquad \alpha_3 \sim \tau_\theta t^4 \left[ B_1' \frac{1}{h^2} + \frac{B_2'}{t^2} (c_2 - 1) \right], \tag{6.26}$$

where $A_1'$, $A_2'$, $B_1'$, $B_2'$ are independent of $t$ and $h$. Comparing (6.26) with (6.12) it is observed that the last term in $\alpha_1$, $\alpha_2$ does not vanish when $c_2 = 1$, contrary to what happens for $\beta_1$, $\beta_2$. Thus, when $t \to 0$ we have that $\alpha_1,\ \alpha_2 = \mathcal{O}(\tau_\theta t^4)$ and $\alpha_3 = \mathcal{O}(\tau_\theta t^4 h^{-2})$, as claimed earlier.

Therefore, we have proved that there is a positive constant $C$ for which the following inequality holds:

$$B_{\text{stab}}(\mathbf{u}_h, \mathbf{v}_h) \geqslant C |\!|\!| \mathbf{u}_h |\!|\!|^2. \tag{6.27}$$

It is also easy to check that

$$|\!|\!| \mathbf{v}_{h1} |\!|\!|^2 \leqslant \tau_\theta^2 \frac{C_{\text{inv}}^4}{h^4} (\alpha_1 + \alpha_2) \left( k_1^2 \|\nabla \boldsymbol{\theta}_h\|_K^2 + k_2^2 \|\nabla \cdot \boldsymbol{\theta}_h\|_K^2 \right) + \tau_\theta^2 \varepsilon^{-2} \frac{C_{\text{inv}}^2}{h^2} (\alpha_1 + \alpha_2) \|\boldsymbol{\gamma}_h\|_K^2 \leqslant C |\!|\!| \mathbf{u}_h |\!|\!|^2, \tag{6.28}$$

$$|\!|\!| \mathbf{v}_{h2} |\!|\!|^2 \leqslant \tau_w^2 \varepsilon^{-2} \alpha_3 \frac{C_{\text{inv}}^4}{h^4} \|\boldsymbol{\gamma}_h\|_K^2 \leqslant C |\!|\!| \mathbf{u}_h |\!|\!|^2, \tag{6.29}$$

and therefore $|\!|\!| \mathbf{v}_h |\!|\!|^2 \leqslant C |\!|\!| \mathbf{u}_h |\!|\!|^2$. From this result and (6.27) it follows that for each $\mathbf{u}_h \in \mathcal{X}_h$ there exists $\mathbf{v}_h \in \mathcal{X}_h$ such that $B_{\text{stab}}(\mathbf{u}_h, \mathbf{v}_h) \geqslant C |\!|\!| \mathbf{u}_h |\!|\!| \, |\!|\!| \mathbf{v}_h |\!|\!|$, from where the theorem follows. □

Once the stability is established, a standard procedure follows to prove convergence. There are two preliminary lemmas that are needed to achieve it, concerning the consistency and the interpolation error.

**Lemma 6.2 (Consistency).** *Let $\mathbf{u} \in \mathcal{X}$ be the solution of the continuous problem and $\mathbf{u}_h \in \mathcal{X}_h$ the FE solution of* (6.5)*. If $\mathbf{u}$ is regular enough so that $B_{\text{stab}}(\mathbf{u}, \mathbf{v}_h)$ is well defined, then*

$$B_{\text{stab}}(\mathbf{u} - \mathbf{u}_h, \mathbf{v}_h) = 0, \quad \forall \mathbf{v}_h \in \mathcal{X}_h. \tag{6.30}$$

*Proof.* Since the stabilization terms are residual based and the Galerkin method does not contribute to the consistency error, the lemma is satisfied by construction. □

The following lemma concerns an interpolation error in terms of the working norm $|\!|\!| \cdot |\!|\!|$ and the bilinear

form $B_{\text{stab}}$. Let $\mathcal{W}_h$ be a generic FE space of degree $k_v$. The interpolation error $\epsilon_i(v)$ for any function $v \in H^{k'_v+1}(\Omega)$ for $i = 0, 1$ is defined as follows

$$\inf_{v_h \in \mathcal{W}_h} \sum_K \|v - v_h\|_{H^i(K)} \leqslant C h^{k''_v+1-i} \sum_K \|v\|_{H^{k''_v+1}(K)} =: \epsilon_i(v), \tag{6.31}$$

where $k''_v = \min(k_v, k'_v)$. Also consider $\tilde{v}_h$ to be the best approximation of $v$ in $\mathcal{W}_h$. Note that $\epsilon_0(v) = h\epsilon_1(v)$. In particular, the notation will be $v = \boldsymbol{\theta}$ for the rotations and $v = w$ for the deflection, with orders of interpolation $k_\theta$ and $k_w$, respectively.

The error function of the method will be proven to be:

$$E(h) := \left(\sqrt{k_1} + \sqrt{k_2}\right) \epsilon_1(\boldsymbol{\theta}) + \frac{1}{\sqrt{\varepsilon}} \epsilon_0(\boldsymbol{\theta}) + \frac{1}{\sqrt{\varepsilon}} \epsilon_1(w). \tag{6.32}$$

**Lemma 6.3 (Interpolation error).** *Let $\mathbf{u} \in \mathcal{X}$ be the continuous solution, assumed to be regular enough, and $\tilde{\mathbf{u}}_h \in \mathcal{X}_h$ its best FE approximation. Then the following inequalities hold:*

$$B_{\text{stab}}(\mathbf{u} - \tilde{\mathbf{u}}_h, \mathbf{v}_h) \leqslant C E(h) |||\mathbf{v}_h|||, \tag{6.33}$$
$$|||\mathbf{u} - \tilde{\mathbf{u}}_h||| \leqslant C E(h). \tag{6.34}$$

*Proof.* Let us prove (6.34). Consider the definition of the working norm (6.13); it can be easily checked that

$$|||\mathbf{u} - \tilde{\mathbf{u}}_h|||^2 \leqslant C \left[\alpha_1 \epsilon_1^2(\boldsymbol{\theta}) + \alpha_2 \epsilon_1^2(\boldsymbol{\theta}) + \alpha_3 \epsilon_1^2(w) + \alpha_3 \epsilon_0^2(\boldsymbol{\theta})\right], \tag{6.35}$$

from where (6.34) follows using (5.16) for the expression of the stabilization parameters and (6.23)-(6.25) for the expression of $\alpha_i$, $i = 1, 2, 3$.

Then consider $\boldsymbol{e}_u = \mathbf{u} - \tilde{\mathbf{u}}_h = [\boldsymbol{e}_\theta, e_w]$, where $\boldsymbol{e}_\theta = \boldsymbol{\theta} - \tilde{\boldsymbol{\theta}}_h$ and $e_w = w - \tilde{w}_h$; the proof of (6.33) is as follows:

$$\begin{aligned}
B_{\text{stab}}(\boldsymbol{e}_u, \mathbf{v}_h) =& k_1 (\nabla \boldsymbol{e}_\theta, \nabla \boldsymbol{\phi}_h) + k_2 (\nabla \cdot \boldsymbol{e}_\theta, \nabla \cdot \boldsymbol{\phi}_h) + \frac{1}{\varepsilon} (\nabla e_w - \boldsymbol{e}_\theta, \nabla v_h - \boldsymbol{\phi}_h) \\
&+ \tau_\theta \sum_K \left\langle P_\theta^\perp \left[ k_1 \Delta \boldsymbol{e}_\theta + k_2 \nabla(\nabla \cdot \boldsymbol{e}_\theta) + \frac{1}{\varepsilon} (\nabla e_w - \boldsymbol{e}_\theta) \right], P_\theta^\perp \left[ -k_1 \Delta \boldsymbol{\phi}_h - k_2 \nabla(\nabla \cdot \boldsymbol{\phi}_h) - \frac{1}{\varepsilon} \boldsymbol{\gamma}_h \right] \right\rangle_K \\
&+ \tau_w \sum_K \left\langle P_w^\perp \left[ \frac{1}{\varepsilon} \nabla \cdot (\nabla e_w - \boldsymbol{e}_\theta) \right], P_w^\perp \left[ -\frac{1}{\varepsilon} \nabla \cdot \boldsymbol{\gamma}_h \right] \right\rangle_K \\
\leqslant& \sqrt{k_1} \|\nabla \boldsymbol{e}_\theta\| \sqrt{k_1} \|\nabla \boldsymbol{\phi}_h\| + \sqrt{k_2} \|\nabla \cdot \boldsymbol{e}_\theta\| \sqrt{k_2} \|\nabla \cdot \boldsymbol{\phi}_h\| + \frac{1}{\sqrt{\varepsilon}} \|\nabla e_w - \boldsymbol{e}_\theta\| \frac{1}{\sqrt{\varepsilon}} \|\boldsymbol{\gamma}_h\| \\
&+ \left( \tau_\theta \frac{k_1}{h} \|\nabla \boldsymbol{e}_\theta\| + \tau_\theta \frac{k_2}{h} \|\nabla \cdot \boldsymbol{e}_\theta\| + \frac{\tau_\theta}{\varepsilon} (\|\nabla e_w\| + \|\boldsymbol{e}_\theta\|) \right) \left( k_1 \frac{C_{\text{inv}}}{h} \|\nabla \boldsymbol{\phi}_h\| \right. \\
&\left. + k_2 \frac{C_{\text{inv}}}{h} \|\nabla \cdot \boldsymbol{\phi}_h\| + \frac{1}{\varepsilon} \|\boldsymbol{\gamma}_h\| \right) + \left( \tau_w \frac{1}{\varepsilon} \frac{1}{h} \|\nabla e_w\| + \tau_w \frac{1}{\varepsilon} \|\nabla \cdot \boldsymbol{e}_\theta\| \right) \frac{C_{\text{inv}}}{\varepsilon h} \|\boldsymbol{\gamma}_h\| \\
\leqslant& \left[ \left( k_1 + \tau_\theta k_1^2 \frac{C_{\text{inv}}}{h^2} \right) \|\nabla \boldsymbol{e}_\theta\| + \tau_\theta k_1 k_2 \frac{C_{\text{inv}}}{h^2} \|\nabla \cdot \boldsymbol{e}_\theta\| + \tau_\theta \frac{k_1}{\varepsilon} \frac{C_{\text{inv}}}{h} \|\nabla e_w\| \right. \\
&\left. + \tau_\theta \frac{k_1}{\varepsilon} \frac{C_{\text{inv}}}{h^2} \|\boldsymbol{e}_\theta\| \right] \|\nabla \boldsymbol{\phi}_h\| + \left[ \tau_\theta k_1 k_2 \frac{C_{\text{inv}}}{h^2} \|\nabla \boldsymbol{e}_\theta\| + \left( k_2 + \tau_\theta k_2^2 \frac{C_{\text{inv}}}{h^2} \right) \|\nabla \cdot \boldsymbol{e}_\theta\| \right. \\
&\left. + \tau_\theta \frac{k_2}{\varepsilon} \frac{C_{\text{inv}}}{h} \|\nabla e_w\| + \tau_\theta \frac{k_2}{\varepsilon} \frac{C_{\text{inv}}}{h^2} \|\boldsymbol{e}_\theta\| \right] \|\nabla \cdot \boldsymbol{\phi}_h\|
\end{aligned}$$

$$
\begin{aligned}
&+\left[\tau_\theta\frac{k_1}{\varepsilon h}\|\nabla \boldsymbol{e}_\theta\|+\tau_\theta\frac{k_2}{\varepsilon h}\|\nabla\cdot\boldsymbol{e}_\theta\|+\left(\frac{1}{\varepsilon}+\frac{\tau_\theta}{\varepsilon^2}+\tau_w\frac{C_{\text{inv}}}{\varepsilon^2h^2}\right)\left(\|\nabla e_w\|+\|\boldsymbol{e}_\theta\|\right)\right]\|\boldsymbol{\gamma}_h\|\\
\leqslant& C\left[k_1\|\nabla\boldsymbol{e}_\theta\|+k_2\|\nabla\cdot\boldsymbol{e}_\theta\|+\frac{h}{\varepsilon}\|\nabla e_w\|+\frac{h}{\varepsilon}\|\boldsymbol{e}_\theta\|\right]\left(\|\nabla\boldsymbol{\phi}_h\|_K+\|\nabla\cdot\boldsymbol{\phi}_h\|+\frac{1}{h}\|\boldsymbol{\gamma}_h\|\right)\\
\leqslant& C\left[\left(\sqrt{k_1}+\sqrt{k_2}\right)\epsilon_1(\boldsymbol{\theta})+\frac{1}{\sqrt{\varepsilon}}\epsilon_0(\boldsymbol{\theta})+\frac{1}{\sqrt{\varepsilon}}\epsilon_1(w)\right]\left(\sqrt{\alpha_1}\,\|\nabla\boldsymbol{\phi}_h\|+\sqrt{\alpha_2}\,\|\nabla\cdot\boldsymbol{\phi}_h\|+\sqrt{\alpha_3}\,\|\boldsymbol{\gamma}_h\|\right).
\end{aligned}
\tag{6.36}
$$

All the terms have been organized to see that it is clear that they are all bounded by $CE(h)|||\mathbf{v}_h|||$, from where (6.33) follows. □

With this, it only remains to prove convergence, which proceeds in a standard manner.

**Theorem 6.4 (Convergence).** *Let $\mathbf{u}\in\mathcal{X}$ be the solution of the continuous problem, assumed to be regular enough. There is a positive constant $C$ such that*

$$
|||\mathbf{u}-\mathbf{u}_h||| \leqslant CE(h). \tag{6.37}
$$

*Proof.* Consider $\tilde{\mathbf{u}}_h-\mathbf{u}_h\in\mathcal{X}_h$, where $\tilde{\mathbf{u}}_h$ is the best FE approximation to $\mathbf{u}$. From the inf-sup condition (6.14) it follows that there exists $\mathbf{v}_h\in\mathcal{X}_h$ such that

$$
\begin{aligned}
C|||\tilde{\mathbf{u}}_h-\mathbf{u}_h|||\,|||\mathbf{v}_h||| &\leqslant B_{\text{stab}}(\tilde{\mathbf{u}}_h-\mathbf{u}_h,\mathbf{v}_h)\\
&= B_{\text{stab}}(\tilde{\mathbf{u}}_h-\mathbf{u},\mathbf{v}_h) \qquad (\text{from the consistency (6.30)})\\
&\leqslant CE(h)|||\mathbf{v}_h||| \qquad\qquad (\text{from (6.33)}),
\end{aligned}
$$

from where $|||\tilde{\mathbf{u}}_h-\mathbf{u}_h||| \leqslant CE(h)$. Subsequently, the theorem follows from the triangle inequality $|||\mathbf{u}-\mathbf{u}_h||| \leqslant |||\mathbf{u}-\tilde{\mathbf{u}}_h|||+|||\tilde{\mathbf{u}}_h-\mathbf{u}_h|||$ and the interpolation error estimate (6.34). □

From this result and the expression of the error function in (6.32) it follows that when $t$ is 'large' the optimal combination of interpolation orders for rotations and displacements is $k_\theta=k_w$. However, when $t$ is small, say $t<h$, the best is to take $k_\theta=k_w-1$, since in this case rotations and deflection contribute with the same order of $h$ to the error of the formulation.

## 7 Numerical results

All the examples of this section have been run considering linear continuous interpolation for both rotations and displacements, i.e., $k_\theta=k_w=1$.

### *7.1 Shear-locking*

In this section, the behavior of the ASGS and OSGS formulations is evaluated for the plate and beam problems. From the physical point of view, the formulations must be able to represent thin behavior, or in other words, the effects of shear deformations must become negligible for decreasing thickness. From the numerical point of view, this can be verified if the numerical results are free from shear-locking. This implies that the solution obtained using the Reissner-Mindlin and Timoshenko theories should coincide with the solution of the Kirchhoff and the Euler-Bernoulli beam theory, respectively, for small thicknesses.

To assess this behavior, let us consider a square plate of domain $\Omega = (0, L)^2$ clamped on all its sides and subject to a uniform load $q = 1$ and a cantilever beam of domain $\Omega = (0, L)$ with a point load $P = -1$ at the right end and clamped at the left one. For the beam geometry we define a rectangular cross section of side $b = 1$ and thickness $t$, thus the inertia is $I = bt^3/12$. For the material properties we consider $E = 10^6$ and $\nu = 0.2$ in all cases (SI units can be assumed to fix ideas). The analytical deflection at the center of the plate and at the end of the beam according to the Kirchhoff and Euler-Bernoulli theories are, respectively:

$$w_{\mathrm{K}} = 0.01524 \frac{qL^4(1-\nu^2)}{Et^3}, \qquad w_{\mathrm{E}} = \frac{PL^3}{3EI}. \tag{7.1}$$

For the numerical computations, we consider a mesh of $20 \times 20$ square elements for the plate and 50 linear elements for the beam. The ratio between the deflection obtained numerically from the stabilized formulations and the analytical solutions respect to the thickness is plotted in Fig. 2. Results show that both formulations are able to represent the thin limit behavior.

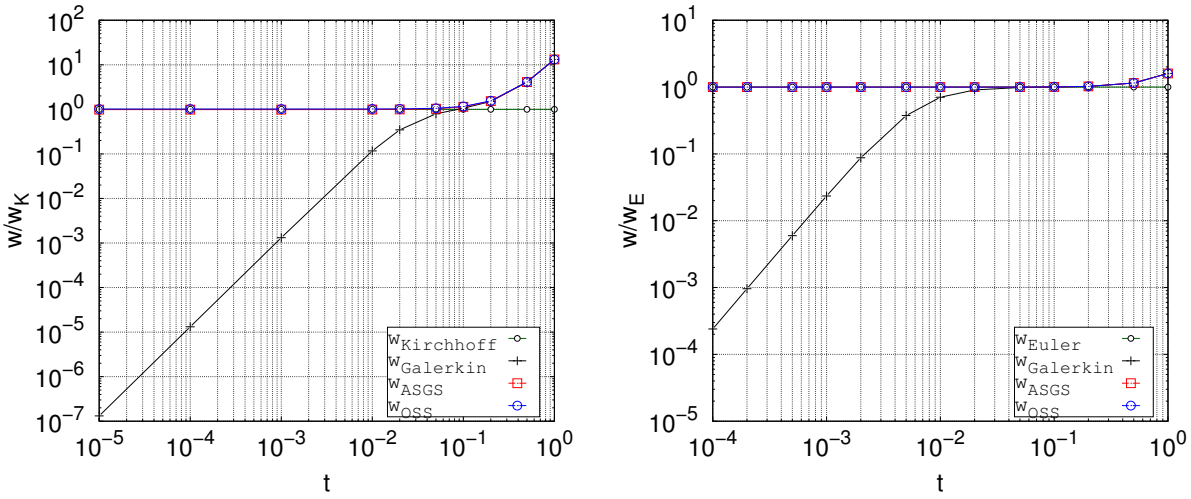


Figure 2: Comparison of deflection $w$ from numerical results vs analytical solutions for different thicknesses of plates (left) and beams (right).

In order to have a reference of the performance of the methods proposed, the behavior of ASGS and OSGS formulations is compared to that obtained by the reduced integration of the shear terms, i.e., those that involve rotations. In the case of beams, Fig. 3 shows that both ASGS and OSGS converge slightly faster to the analytical solution compared to reduced integration; however, the convergence test presented below shall depict the true nature of the formulations discussed in the present work.

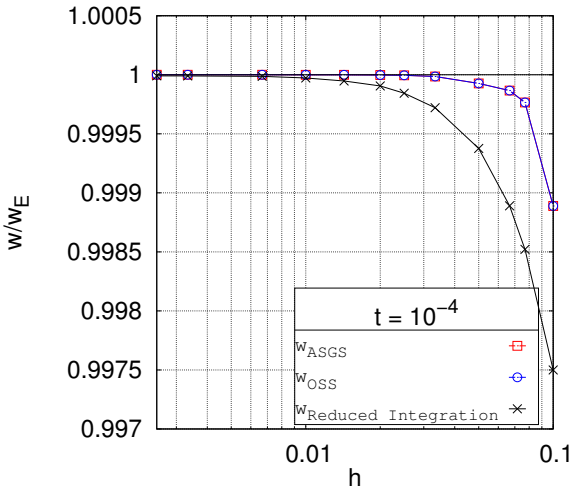


Figure 3: Comparison of relative deflection $w$ from numerical results vs analytical solutions for different element sizes.

### *7.2 Convergence tests*

#### *7.2.1. Convergence for beams*

To assess the convergence of the stabilized Timoshenko beam formulation, consider a beam oriented in the $x$ direction clamped at both sides, a homogeneous load $q = 1$ on its entire length $L = 1$, and the same material and geometrical properties as in the previous beam example. Since the formulation has to be able to represent the thin behavior, the solutions of the numerical method is compared to the analytical solution of the Euler-Bernoulli beam theory:

$$\theta_z(x) = \frac{qx}{12EI}(L-x)(1-2x), \qquad w(x) = \frac{qx^2}{24EI}(L-x)^2.$$

The problem then is numerically solved for decreasing element sizes $h$, thicknesses of $t = 10^{-4}, 10^{-5}$ which correspond to slenderness ratios of $L/t = 10^4, 10^5$, respectively, and the error is evaluated in the $L^2$ norm. For comparison purposes, results are shown for the standard Galerkin, ASGS and OSGS formulations, as presented in Fig. 4. Results show that deflections and rotations are optimally convergent respect to the element size using any of the two stabilized formulations.

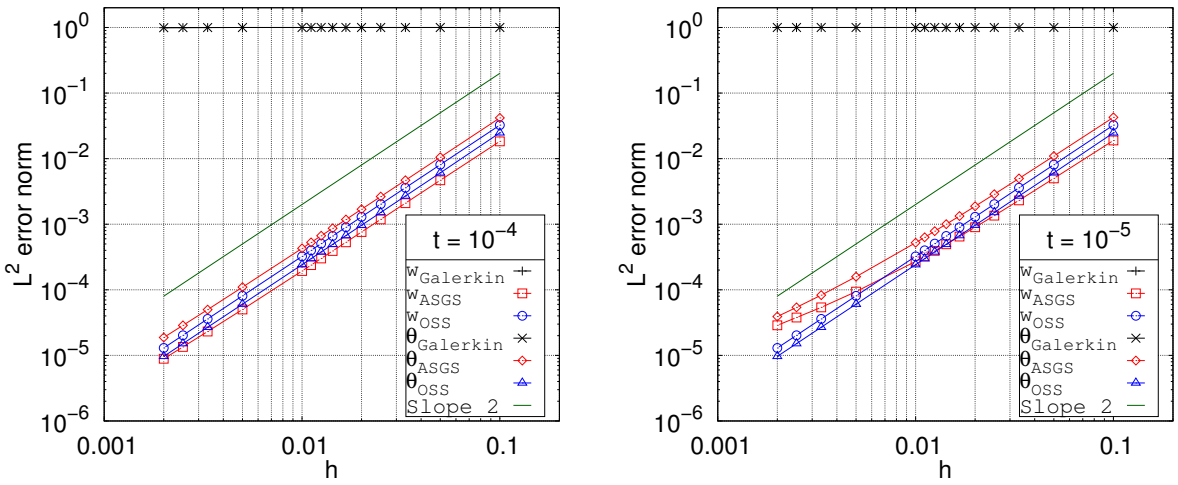


Figure 4: Beam $L^2$-error norm for Galerkin, ASGS and OSGS formulations for $L/t = 10^4$ (left) and $L/t = 10^5$ (right).

For the numerical tests, the stabilization constants chosen for the ASGS formulation are $c_1 = c_3 = 12$, as found in section 5. In the case of the OSGS formulation, the values of the constants have no justification from the exact solution, and were chosen by testing different values. Nevertheless, this selection is not arbitrary; it is known that the zero shear constraint is difficult to handle, and selecting small values of $c_1$ can alleviate it. Under this assumption, it was found that values of $c_1 \leqslant 10^{-3}$ have to be used to obtain optimally convergent results. Recall that for linear elements the only condition needed for stability is that $c_1 > 0$, as discussed in section 6.

One important aspect of a locking-free formulation is that its convergence should be independent of the thickness, at least to some degree. To assess this dependence, the convergence curves of the displacements are plotted for different thicknesses. As presented in Fig. 5, the ASGS formulation becomes noticeable dependent on the thickness for low enough values, while the OSGS formulation shows a robust behavior since it is almost independent of it.

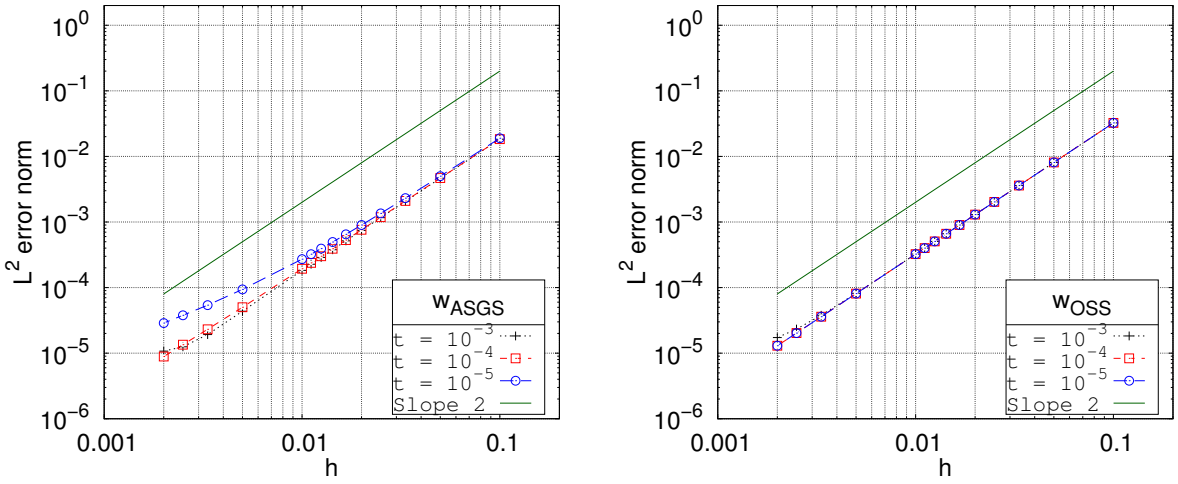


Figure 5: Beam displacement $L^2$-error norm for different thicknesses, ASGS (left) and OSGS (right).

*7.2.2. Convergence for plates*

To assess the convergence of the stabilized Reissner-Mindlin plate formulation, consider a square plate of domain $\Omega = (0, L)^2$ clamped on all sides. The test is computed applying a load that follows the function proposed in [19]:

$$q(x,y) = \frac{E}{12(1-\nu^2)}[12y(y-1)(5x^2-5x+1)(2y^2(y-1)^2 + x(x-1)(5y^2-5y+1)) \\ + 12x(x-1)(5y^2-5y+1)(2x^2(x-1)^2 + y(y-1)(5x^2-5x+1))],$$

for which the exact solutions of displacements and rotations are given by

$$w(x,y) = \frac{x^3y^3}{3t^3}(x-1)^3(y-1)^3 - \frac{2}{5t(1-\nu)}[y^3(y-1)^3x(x-1)(5x^2-5x+1) \\ + x^3(x-1)^3y(y-1)(5y^2-5y+1)],$$
$$\theta_x(x,y) = \frac{y^3x^2}{t^3}(y-1)^3(x-1)^2(2x-1),$$
$$\theta_y(x,y) = \frac{x^3y^2}{t^3}(x-1)^3(y-1)^2(2y-1).$$

The load, displacement and rotation fields are showed graphically in Fig. 6.

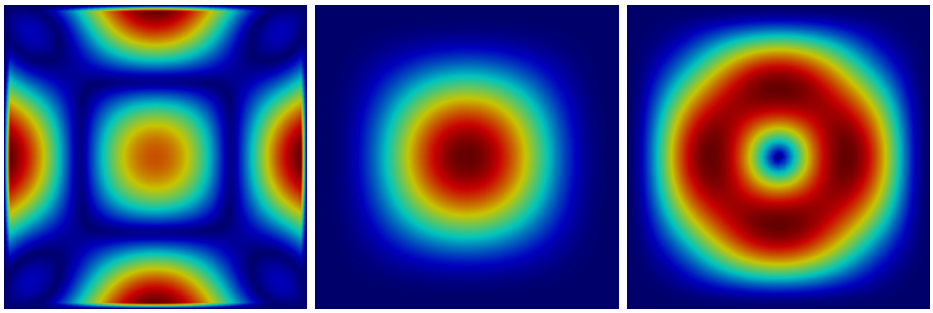

Figure 6: Applied Load (left) and numerical solutions of displacement (center) and norm of the rotation vector (right).

The problem then is solved for decreasing element sizes $h$, considering a constant thicknesses of $t = 10^{-4}$, and $10^{-5}$ which correspond to slenderness ratios of $L/t = 10^4$ and $10^5$, respectively, and the error is evaluated in the $L^2$ norm. Numerical tests have been computed to evaluate which stabilization parameters are best suited to obtain optimal convergence. In regard of this, the only constant that must remain fixed is $c_2 = 1$, as proven in the convergence analysis. As for the other constants, optimal values have not been found for the ASGS formulation, while in the OSGS formulation $c_1 \leqslant 10^{-3}$ has proven to give good results. As presented in Fig. 7 for the OSGS formulation, results prove to converge optimally respect to the element size.

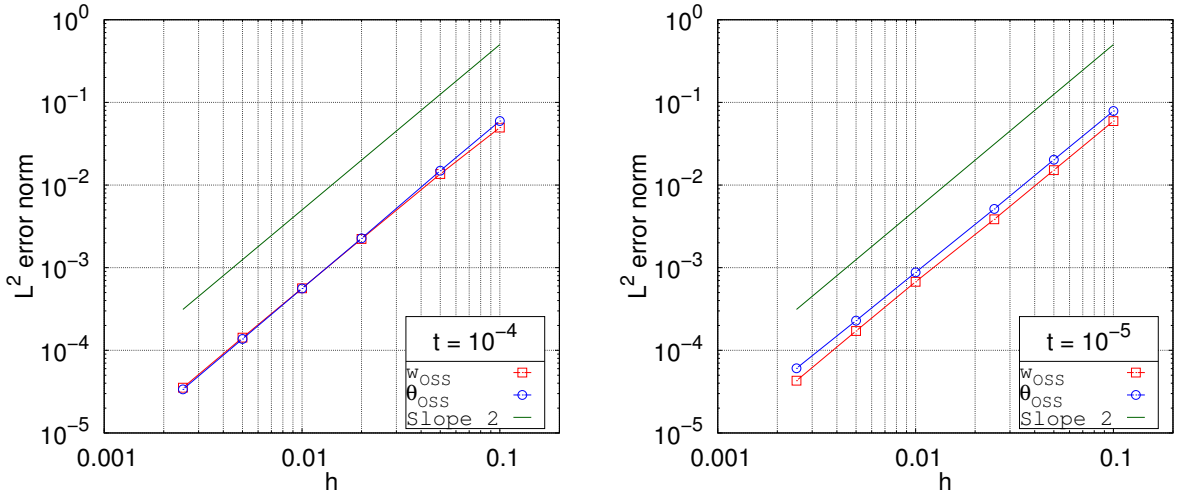


Figure 7: Plates $L^2$-error norm for OSGS formulation, for $L/t = 10^4$ (left) and $L/t = 10^5$ (right).

It is important to note that the constants $c_3$ and $c_4$, which are associated to $\tau_w$, have little impact on the solution. This is explained in detail in subsection 7.3. Recall that the theory does not predict locking-free convergence for the ASGS formulation. Lastly, the dependency of the thickness is evaluated by comparing the $L^2$ error norm for the different thicknesses. As presented in Fig. 8, the accuracy of the solution does not depend on the thickness of the plate.

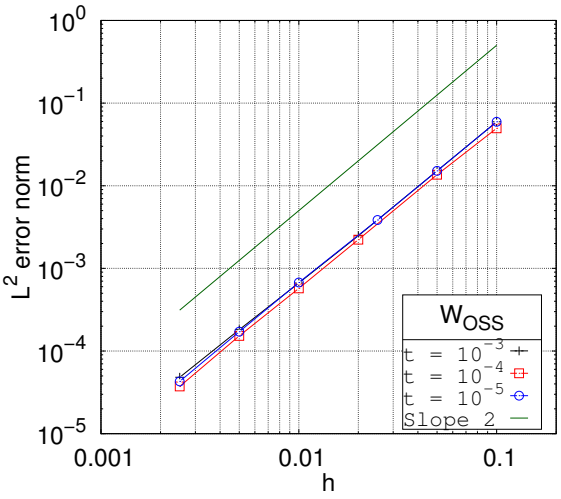


Figure 8: Plate displacement $L^2$-error norm for different thicknesses using OSGS stabilization.

### *7.3 Sensitivity to stabilization constants*

In this subsection, the sensitivity of the numerical solution to the stabilization constants is checked using numerical examples. When evaluating the convergence of the ASGS formulation for beams, the stabilization parameters were set using the constants $c_1 = c_3 = 12$ obtained from the elastic equations, which is not possible in plates. Even though in the beam case the constants are well defined for the ASGS formulation, it is important to check the performance of both ASGS and OSGS formulations for any set of constants.

To address this, consider the same clamped beam with uniform load discussed previously in this section, the problem is solved repeatedly for different values of $c_1$ and $c_3$, which are modified independently.

In the ASGS case, for the slenderness ratio of $L/t = 10^5$ several values of the stabilization constants are tested. The constant $c_1$ is tested for slightly perturbed values, namely $12 \pm 0.1$ and $c_3$ is tested for a set of values ranged in $[2, 20]$, as shown in Fig. 9. Results show that the best convergence ratio is obtained for $c_1 = c_3 = 12$, however, a slight variation of $c_1$ is enough to lock the problem in a constant error independently of the element size, while $c_3$ allows a more flexible range of working values. The numerical tests confirm that the values obtained from the elastic equations provide the best behavior of the solution, which cannot be found in the case of plates. Regarding this, the convergence ratio curves of the ASGS formulation for plates has the same behavior as the first image in Fig. 9. Since the values of $c_1 = c_3 = 12$ are not valid for plates and the constants that provide optimal convergence were were not found, results as the second image of Fig. 9 can not be replicated.

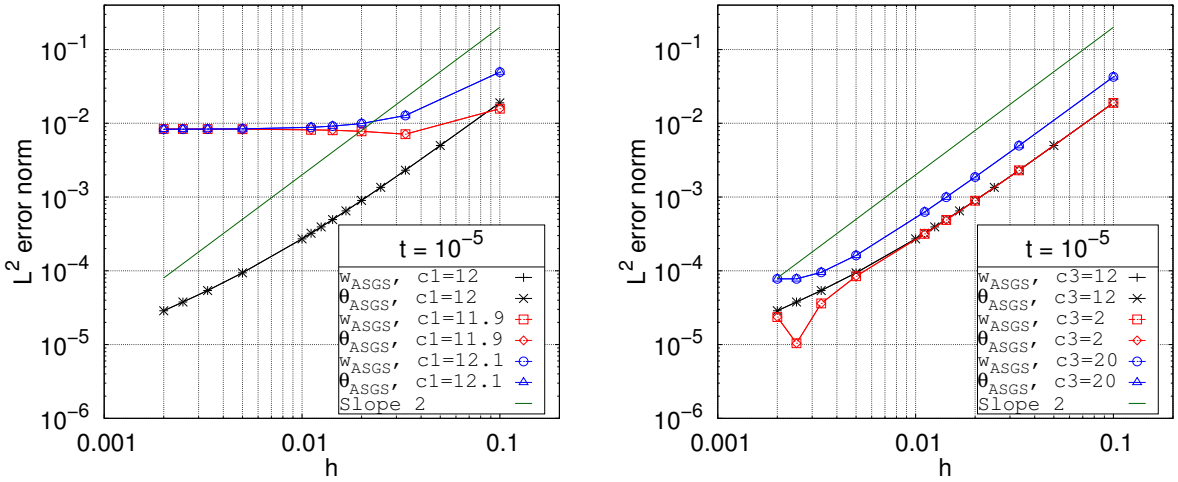


Figure 9: Sensitivity to $c_1$ (left) and $c_3$ (right) in $L2$-error norm, for $L/t = 10^5$.

In the case of the OSGS formulation, the stabilization constants do not have a significant impact on the final solution when $c_1 \leqslant 10^{-3}$. In this regard, the flexibility to choose any value for $c_3$ has to be assessed properly. Let us compute the convergence curves for the same beam case presented above, but this time to compare the results of extreme values of $c_3$, as presented in Fig. 10.

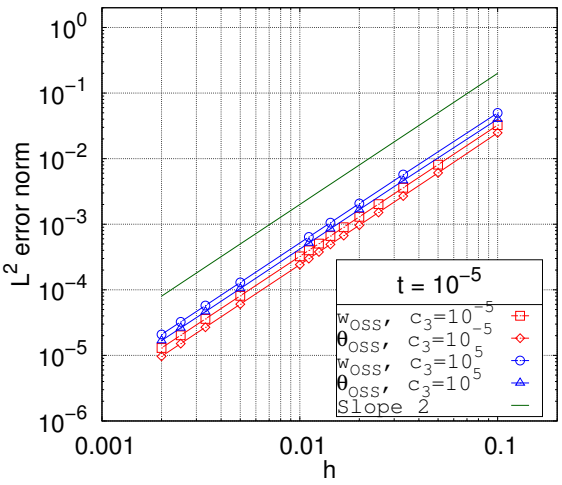


Figure 10: $L2$-error norm for different values of $c_3$, for $L/t = 10^5$.

Results show that the curves are almost identical independently of the value of $c_3$. This is, however, an important feature of the formulation: for high values of $c_3$, the influence of the terms that contain $\tau_w$ is reduced, and in fact, it would be more useful not to consider them at all. From the practical point of view, this is equivalent to remove the projection of the force equilibrium equation, or $\xi_w$, from the formulation, lowering the total number of degrees of freedom. This response to stabilization constants behaves exactly the same for plates as well, and the fact that the number of degrees of freedom of the formulation can be reduced is specially useful for lowering the cost of computations.

### *7.4 Applied examples*

Three numerical examples are solved to illustrate the performance of the OSGS formulation with respect to the Galerkin formulation. The cases presented below are just a few of the many examples found in the literature. Results presented show that the OSGS formulation is free of locking and converges to the exact solution much faster than the locked solution obtained using the Galerkin approach. This behavior is independent of the thickness of the plate, which is consistent with the convergence tests presented in 7.2.2.

#### *7.4.1. Clamped circular plate with uniform load*

Consider a clamped circular plate of radius $R = 5$ loaded with an uniform load of $q = 1$. The geometry, mesh, and boundary conditions are set up as in standard manner described in the literature [38, 39, 40, 41], the solution of circular loaded plates set with different boundary conditions are described in [42]. Due to the symmetry of the case, only a quarter of the geometry is modelled and symmetry boundary conditions are set in both straight sides. The mesh structure, which is built in three patches of square elements, and the deformed configuration are illustrated in Fig. 11.

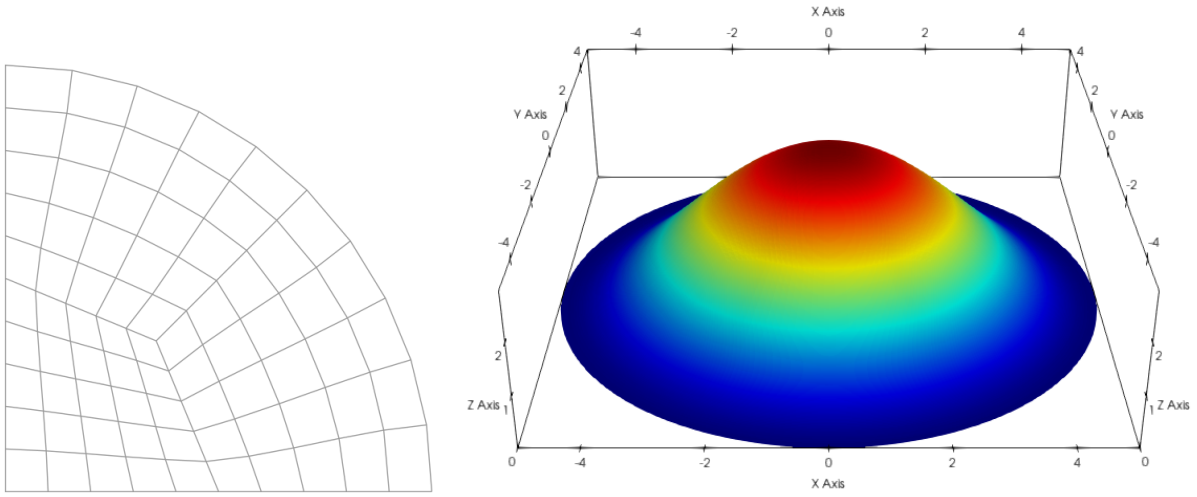


Figure 11: Clamped circular plate with uniform load: Mesh (left) and deformed configuration (right).

Cases are computed for two different thicknesses: $t = 0.1$ and $t = 0.01$ which correspond to slenderness ratios of $R/t = 50$ and $R/t = 500$, respectively. These values are chosen to test cases with high shear-locking effects. For the assessment, the displacements are tracked at the center of the plate ($R = 0$), where they reach their maximum values. Results are shown in Fig.12.

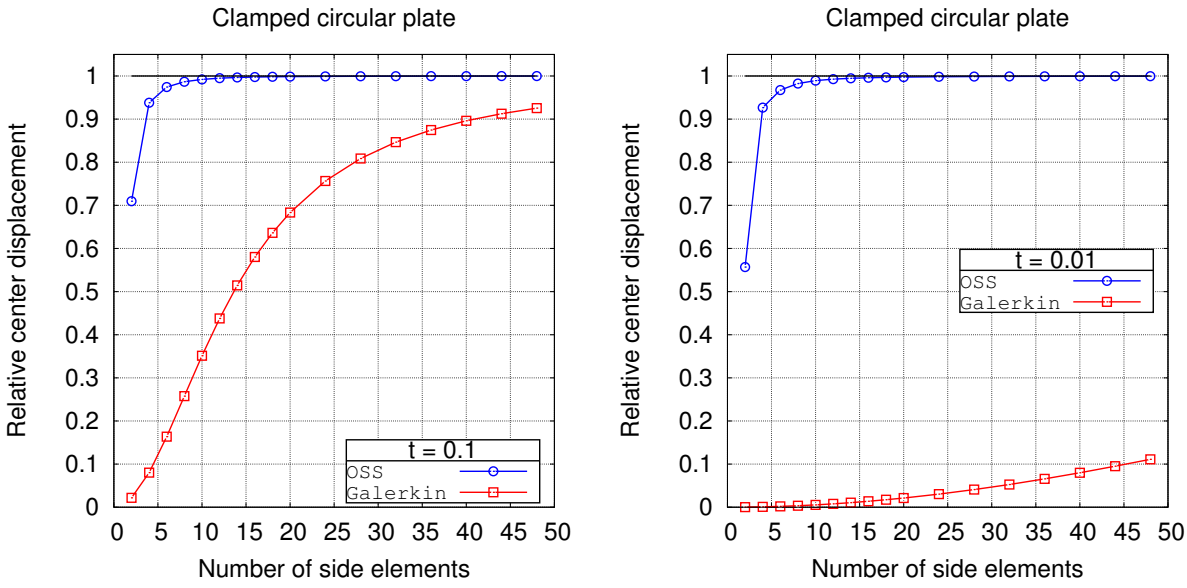


Figure 12: Clamped circular plate with uniform load: relative maximum displacements for cases $t = 0.1$ (left) and $t = 0.01$ (right).

*7.4.2. Simply supported annular plate with uniform load*

Consider a simply supported annular plate of inner radius of $R_i = 1.5$ and outter radius $R_o = 5$, which again correspond to slenderness ratios of $R_o/t = 50$ and $R_o/t = 500$, respectively, and loaded with an uniform load of $q = 1$. The solution of loaded annular plate problems are also described in [42]. As in the previous case, only a quarter of the geometry is needed and symmetry boundary conditions are set in the

straight sides. The mesh, which consists square elements aligned in the radial direction, and the deformed configurations are illustrated in Fig. 13.

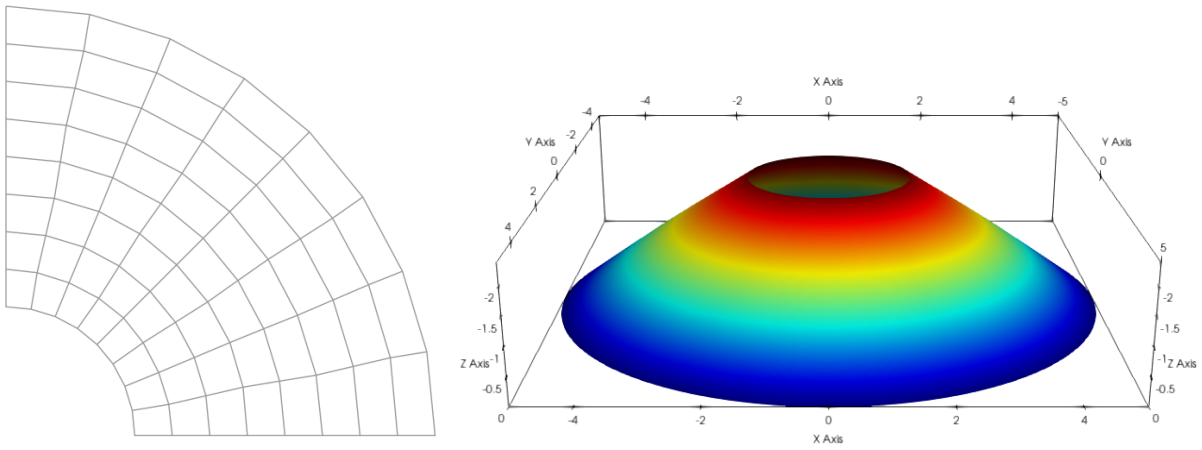


Figure 13: Simply supported annular plate with uniform load: Mesh (left) and deformed configuration (right).

The cases are computed using thicknesses of $t = 0.1$ and $t = 0.01$ for the same reason as the previous case. In this example the displacements are tracked at the inner radius of the plate, where they reach their maximum values. Results are shown in Fig. 14.

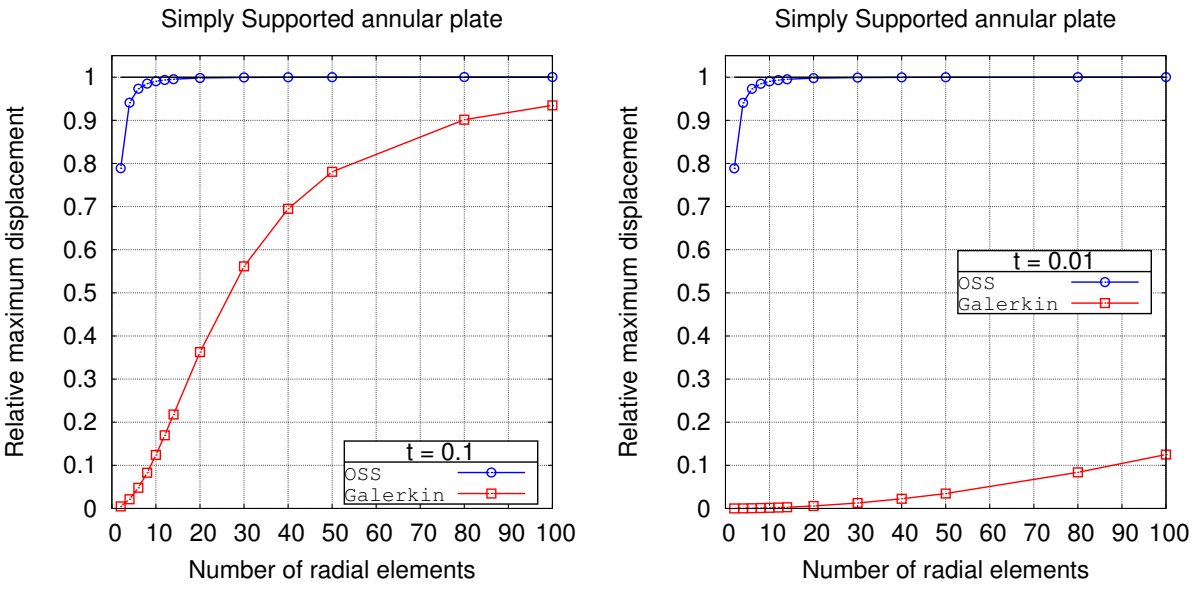


Figure 14: Simply supported annular plate with uniform load: relative maximum displacements for cases $t = 0.1$ (left) and $t = 0.01$ (right).

### *7.4.3. Cantilever plate with hole*

The last case consists in a cantilever plate loaded with an uniform load of $q = 1$, clamped in the wider straight side. The geometry and mesh are illustrated in Fig. 15. The mesh is divided in four patches of four sides each, so that the mesh refinements depend only on the number of elements set in each side.

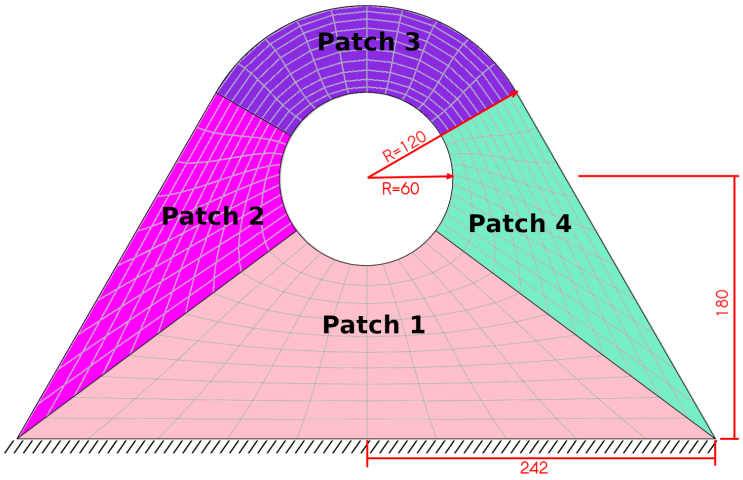


Figure 15: Cantilever plate with hole: geometry and mesh.

The cases are computed using thicknesses of $t = 20$ and $t = 5$, which correspond to slenderness ratios of $L/t = 15$ and $L/t = 60$, respectively, and displacements are tracked at the opposite end to the clamped side, where the displacement reach their maximum value, the deformed geometry is illustrated in Fig. 16. In the case of $t = 20$, results converge to $7.4341 \cdot 10^{-4}$ similar to those presented in [43]. In the more slender case of $t = 5$ the result converges to 0.046546 with mesh refinement. Note that since it is a linear elastic problem, result are proportional to the cube of the thickness, which is $(20/5)^3 = 64$, with respect to the known solution.

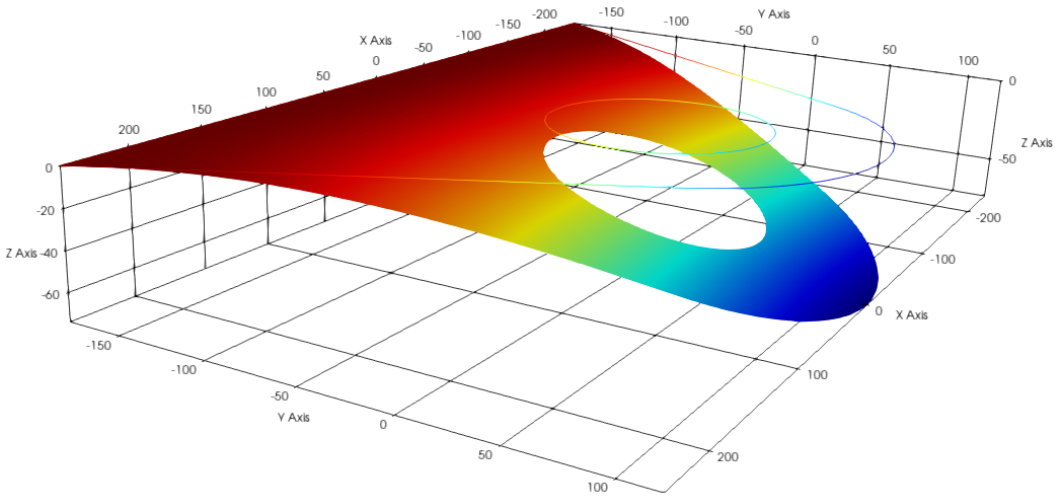


Figure 16: Cantilever plate with hole: deformed geometry.

Results obtained for both thicknesses, including the comparison of the OSGS and the Galerkin formulations are shown in Fig. 17. Note that the converged results are used to compute the relative displacements.

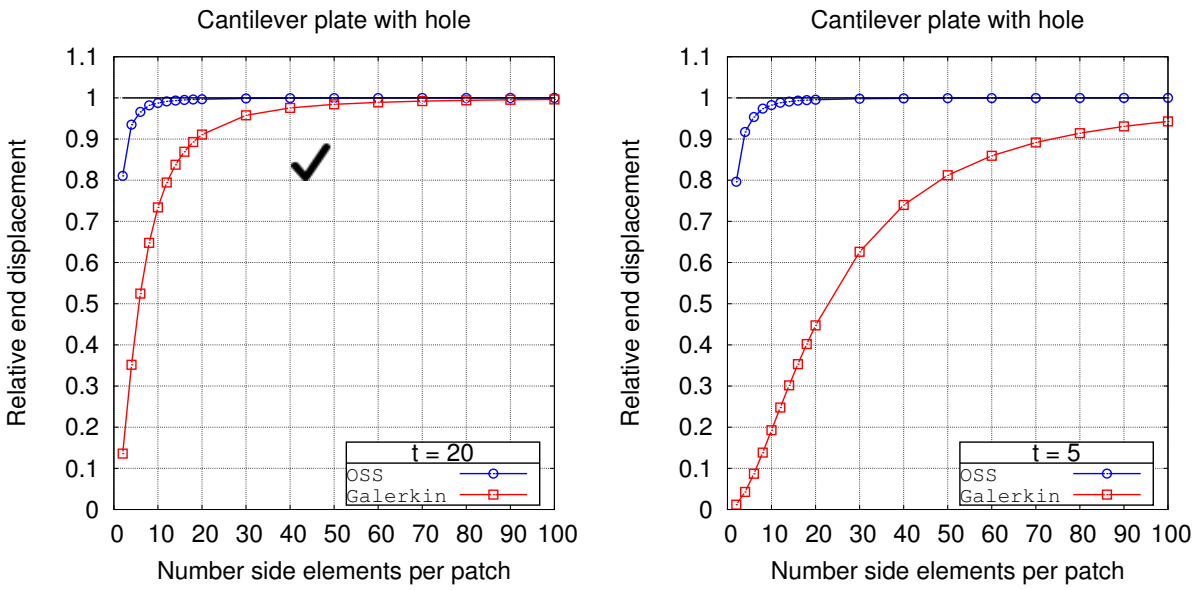


Figure 17: Cantilever plate with hole: relative maximum displacements for cases $t = 20$ (left) and $t = 5$ (right).

## 8 Conclusions

The numerical locking present in standard Galerkin formulations of Reissner-Mindlin plates and Timoshenko beams has been addressed using the Variational Multiscale Method. This, by itself, has the theoretical interest of developing a stable formulation for beams and plates using the same principles that have led to stable and accurate numerical formulations in many other areas of computational engineering. Two particular VMS formulations have been developed, namely, the ASGS and the OSGS methods. It has been shown that the norm in which stability can be proved for the ASGS formulation is not free of locking when $t \to 0$, whereas optimal stability and convergence has been proven for the OSGS approach for arbitrary interpolation of the variables. Nevertheless, for Timoshenko beams there exists a set of algorithmic constants for which the element stiffness matrix of the ASGS formulation coincides with that of the elastic equations, and in this case the method does converge. This, however, has to be considered a singularity rather than a general possibility.

The practical interest of the formulation developed is twofold. First, it has less degrees of freedom than than other formulations that interpolate shear and, furthermore, it can be implemented iteratively so as to use only displacements and rotations as unknowns. And, second, contrary to most locking-free methods, it is applicable to any type of elements, triangles or quads of any order and with arbitrary interpolations for displacements and rotations.

Numerical tests confirm that the theoretical predictions. In particular, the OSGS formulation provides optimally convergent rates, for both displacement and rotations. Moreover, this method is shown to be mildly sensitive to the algorithmic constants. In particular, in the numerical experiments presented it has been unnecessary to activate the stabilization terms corresponding to deflections to obtain optimally

convergent results.

**Acknowledgement**

This work was supported by Vicerrectoría de Investigación, Desarrollo e Innovación (VRIDEI) of the Univeridad de Santiago de Chile, and the National Agency for Research and Development (ANID) Doctorado Becas Chile/2019 - 72200128 of the Government of Chile. R. Codina acknowledges the support received from the ICREA Acadèmia Research Program of the Catalan Government.

[1] J. Rakowski, "The interpretation of the shear locking in beam elements," *Computers & Structures*, vol. 37, no. 5, pp. 769–776, 1990.

[2] E. Oñate, *Structural analysis with the finite element method. Linear statics: volume 2: beams, plates and shells*. Springer Science & Business Media, 2013.

[3] K.-J. Bathe, "The inf–sup condition and its evaluation for mixed finite element methods," *Computers & Structures*, vol. 79, no. 2, pp. 243–252, 2001.

[4] D. Chapelle and K.-J. Bathe, *The finite element analysis of shells-fundamentals*. Springer Science & Business Media, 2010.

[5] R. Durán and E. Liberman, "On mixed finite element methods for the Reissner-Mindlin plate model," *Mathematics of Computation*, vol. 58, no. 198, pp. 561–573, 1992.

[6] C. Lovadina, "Analysis of a mixed finite element method for the Reissner-Mindlin plate problems," *Computer Methods in Applied Mechanics and Engineering*, vol. 163, no. 1-4, pp. 71–85, 1998.

[7] R. Falk and T. Tu, "Locking-free finite elements for the Reissner-Mindlin plate," *Mathematics of Computation*, vol. 69, no. 231, pp. 911–928, 2000.

[8] F. Brezzi, K.-J. Bathe, and M. Fortin, "Mixed-interpolated elements for Reissner–Mindlin plates," *International Journal for Numerical Methods in Engineering*, vol. 28, no. 8, pp. 1787–1801, 1989.

[9] T. J. Hughes and L. P. Franca, "Convergence of transverse shear stresses in the finite element analysis of plates," *Communications in Applied Numerical Methods*, vol. 4, no. 2, pp. 185–187, 1988.

[10] T. J. Hughes and L. P. Franca, "A mixed finite element formulation for Reissner-Mindlin plate theory: Uniform convergence of all higher-order spaces," *Computer Methods in Applied Mechanics and Engineering*, vol. 67, no. 2, pp. 223–240, 1988.

[11] R. Stenberg, "A new finite element formulation for the plate bending problem," *Asymptotic methods for elastic structures*, pp. 209–221, 1995.

[12] P.-S. Lee and K.-J. Bathe, "Development of mitc isotropic triangular shell finite elements," *Computers & Structures*, vol. 82, no. 11-12, pp. 945–962, 2004.

[13] L. B. da Veiga, D. Chapelle, and I. P. Suarez, "Towards improving the MITC6 triangular shell element," *Computers & structures*, vol. 85, no. 21-22, pp. 1589–1610, 2007.

[14] F. Lepe, D. Mora, and R. Rodríguez, "Locking-free finite element method for a bending moment formulation of Timoshenko beams," *Computers & Mathematics with Applications*, vol. 68, no. 3, pp. 118–131, 2014.

[15] M. Toolabi, A. Fallah, P. Baiz, and L. Louca, "Enhanced mixed interpolation xfem formulations for discontinuous Timoshenko beam and Mindlin-Reissner plate," *International Journal for Numerical Methods in Engineering*, vol. 115, no. 6, pp. 714–737, 2018.

[16] B. T. Darrall, G. F. Dargush, and A. R. Hadjesfandiari, "Finite element Lagrange multiplier formulation for size-dependent skew-symmetric couple-stress planar elasticity," *Acta Mechanica*, vol. 225, no. 1, pp. 195–212, 2014.

[17] L. B. da Veiga, D. Mora, and R. Rodríguez, "Numerical analysis of a locking-free mixed finite element method for a bending moment formulation of Reissner-Mindlin plate model," *Numerical Methods for Partial Differential Equations*, vol. 29, no. 1, pp. 40–63, 2013.

[18] F. Brezzi and L. D. Marini, "A nonconforming element for the Reissner–Mindlin plate," *Computers & Structures*, vol. 81, no. 8-11, pp. 515–522, 2003.

[19] C. Chinosi, C. Lovadina, and L. Marini, "Nonconforming locking-free finite elements for Reissner–Mindlin plates," *Computer Methods in Applied Mechanics and Engineering*, vol. 195, no. 25-28, pp. 3448–3460, 2006.

[20] V. M. Calo, N. O. Collier, and A. H. Niemi, "Analysis of the discontinuous Petrov–Galerkin method with optimal test functions for the Reissner–Mindlin plate bending model," *Computers & Mathematics with Applications*, vol. 66, no. 12, pp. 2570–2586, 2014.

[21] T. Führer, C. G. Vera, and N. Heuer, "A locking-free dpg scheme for Timoshenko beams," *Computational Methods in Applied Mathematics*, vol. 21, no. 2, pp. 373–383, 2021.

[22] G. R. Barrenechea, T. P. Barrios, and A. Wachtel, "Stabilised finite element methods for a bending moment formulation of the Reissner-Mindlin plate model," *Calcolo*, vol. 52, no. 3, pp. 343–369, 2015.

[23] J. Videla, S. Natarajan, and S. P. Bordas, "A new locking-free polygonal plate element for thin and thick plates based on Reissner-Mindlin plate theory and assumed shear strain fields," *Computers & Structures*, vol. 220, pp. 32–42, 2019.

[24] P. Peisker, "A multigrid method for Reissner-Mindlin plates," *Numerische Mathematik*, vol. 59, no. 1, pp. 511–528, 1991.

[25] R. Kouhia, "On stabilized finite element methods for the Reissner–Mindlin plate model," *International Journal for Numerical Methods in Engineering*, vol. 74, no. 8, pp. 1314–1328, 2008.

[26] J. Schöberl and R. Stenberg, "Multigrid methods for a stabilized Reissner–Mindlin plate formulation," *SIAM Journal on Numerical Analysis*, vol. 47, no. 4, pp. 2735–2751, 2009.

[27] P. Peisker, W. Rust, and E. Stein, "Iterative solution methods for plate bending problems: multigrid and preconditioned cg algorithm," *SIAM Journal on Numerical Analysis*, vol. 27, no. 6, pp. 1450–1465, 1990.

[28] K.-J. Bathe and E. N. Dvorkin, "A four-node plate bending element based on Mindlin/Reissner plate theory and a mixed interpolation," *International Journal for Numerical Methods in Engineering*, vol. 21, no. 2, pp. 367–383, 1985.

[29] D. Chapelle and R. Stenberg, "An optimal low-order locking-free finite element method for Reissner–Mindlin plates," *Mathematical Models and Methods in Applied Sciences*, vol. 8, no. 03, pp. 407–430, 1998.

[30] D. N. Arnold and F. Brezzi, "Some new elements for the Reissner-Mindlin plate model," *Boundary Value Problems for Partial Differential Equations and Applications*, pp. 287–292, 1993.

[31] M. Bischoff and K.-U. Bletzinger, "Improving stability and accuracy of Reissner–Mindlin plate finite elements via algebraic subgrid scale stabilization," *Computer Methods in Applied Mechanics and Engineering*, vol. 193, pp. 1517–1528, 2004.

[32] T. J. Hughes, "Multiscale phenomena: Green's functions, the dirichlet-to-neumann formulation, subgrid scale models, bubbles and the origins of stabilized methods," *Computer methods in applied mechanics and engineering*, vol. 127, no. 1-4, pp. 387–401, 1995.

[33] T. J. Hughes, G. R. Feijóo, L. Mazzei, and J.-B. Quincy, "The variational multiscale method—A paradigm for computational mechanics," *Computer methods in applied mechanics and engineering*, vol. 166, no. 1-2, pp. 3–24, 1998.

[34] R. Codina, "Stabilization of incompressibility and convection through orthogonal sub-scales in finite element methods," *Computer methods in applied mechanics and engineering*, vol. 190, no. 13-14, pp. 1579–1599, 2000.

[35] R. Codina, S. Badia, J. Baiges, and J. Principe, "Variational multiscale methods in computational fluid dynamics," *Encyclopedia of Computational Mechanics, Second Edition*, pp. 1–28, 2018.

[36] R. Codina, J. Principe, and J. Baiges, "Subscales on the element boundaries in the variational two-scale finite element method," *Computer Methods in Applied Mechanics and Engineering*, vol. 198, no. 5-8, pp. 838–852, 2009.

[37] R. Codina, "On stabilized finite element methods for linear systems of convection–diffusion-reaction equations," *Computer Methods in Applied Mechanics and Engineering*, vol. 188, no. 1-3, pp. 61–82, 2000.

[38] Y. Shang, S. Cen, C.-F. Li, and X.-R. Fu, "Two generalized conforming quadrilateral Mindlin–Reissner plate elements based on the displacement function," *Finite Elements in Analysis and Design*, vol. 99, pp. 24–38, 2015.

[39] L. Yunhua and A. Eriksson, "An alternative assumed strain method," *Computer Methods in Applied Mechanics and Engineering*, vol. 178, no. 1-2, pp. 23–37, 1999.

[40] D. Ribarić and G. Jelenić, "Higher-order linked interpolation in quadrilateral thick plate finite elements," *Finite Elements in Analysis and Design*, vol. 51, pp. 67–80, 2012.

[41] S. Cen, Y. Shang, C.-F. Li, and H.-G. Li, "Hybrid displacement function element method: a simple hybrid-Trefftz stress element method for analysis of Mindlin–Reissner plate," *International Journal for Numerical Methods in Engineering*, vol. 98, no. 3, pp. 203–234, 2014.

[42] W. C. Young, R. G. Budynas, and A. M. Sadegh, *Roark's formulas for stress and strain*. McGraw-Hill Education, 2012.

[43] X. Du, G. Zhao, and W. Wang, "Nitsche method for isogeometric analysis of reissner–mindlin plate with non-conforming multi-patches," *Computer Aided Geometric Design*, vol. 35, pp. 121–136, 2015.